

---

# Multi-Class Uncertainty Calibration via Mutual Information Maximization-based Binning

---

Kanil Patel<sup>\*1,2</sup>, William Beluch<sup>1</sup>, Bin Yang<sup>2</sup>, Michael Pfeiffer<sup>1</sup>, and Dan Zhang<sup>1</sup>

<sup>1</sup>Bosch Center for Artificial Intelligence, Renningen, Germany

<sup>2</sup>Institute of Signal Processing and System Theory, University of Stuttgart, Stuttgart, Germany

## Abstract

Post-hoc calibration is a common approach for providing high-quality confidence estimates of deep neural network predictions. Recent work has shown that widely used scaling methods underestimate their calibration error, while alternative Histogram Binning (HB) methods with verifiable calibration performance often fail to preserve classification accuracy. In the case of multi-class calibration with a large number of classes  $K$ , HB also faces the issue of severe sample-inefficiency due to a large class imbalance resulting from the conversion into  $K$  one-vs-rest class-wise calibration problems. The goal of this paper is to resolve the identified issues of HB in order to provide verified and calibrated confidence estimates using only a small holdout calibration dataset for bin optimization while preserving multi-class ranking accuracy. From an information-theoretic perspective, we derive the *I-Max* concept for binning, which maximizes the mutual information between labels and binned (quantized) logits. This concept mitigates potential loss in ranking performance due to lossy quantization, and by disentangling the optimization of bin edges and representatives allows simultaneous improvement of ranking and calibration performance. In addition, we propose a *shared class-wise* (sCW) binning strategy that fits a single calibrator on the merged training sets of all  $K$  class-wise problems, yielding reliable estimates from a small calibration set. The combination of sCW and I-Max binning outperforms the state of the art calibration methods on various evaluation metrics across different benchmark datasets and models, even when using only a small set of calibration data, e.g. 1k samples for ImageNet.

## 1 Introduction

Despite great ability in learning discriminative features, deep neural network (DNN) classifiers often make over-confident predictions. This can lead to potentially catastrophic consequences in safety critical applications, e.g., medical diagnosis and perception tasks in autonomous driving. A perfectly calibrated classifier should be correct  $p\%$  of the time on cases to which it assigns  $p\%$  confidence, and this mismatch can be measured through the Expected Calibration Error (ECE).

Since the pioneering work of Guo et al. [5], scaling methods have been widely acknowledged as an efficient post-hoc calibration solution for modern DNNs. Recently, [13, 26] showed that the ECE metric [5] is underestimated, and more critically, that it fails to provide a verifiable measure for *scaling methods*, owing to the bias/variance tradeoff in the evaluation error. To estimate ECE from a set of evaluation samples, the prediction probabilities made by scaling methods need to be quantized/binning; this discrete approximation of a continuous function introduces a bias into the empirical estimate of ECE. Increasing the number of evaluation bins reduces this bias, as the quantization error is smaller, however, the estimation of the ground truth correctness begins to suffer from high variance. Fig. 1-a) shows that the empirical ECE estimates of both the raw network

---

<sup>\*</sup>firstname.lastname@de.bosch.com

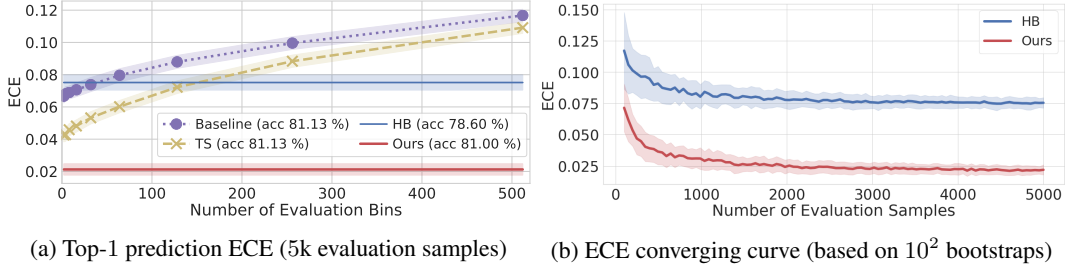


Figure 1: (a) Temperature scaling (TS) [5], equally sized-histogram binning (HB) [29], and our proposal, i.e., sCW I-Max binning are compared for post-hoc calibrating a CIFAR100 (WRN) classifier. (b) Binning offers a reliable ECE measure as the number of evaluation samples increases.

outputs and the temperature scaling method (TS) [5] vary over the number of evaluation bins. It is yet unclear how to choose the optimal number of bins so that the estimation error is minimized for the given number of evaluation samples. In other words, which ECE estimate best reflects the true calibration error remains an open question, rendering the empirical ECE estimation of *scaling methods* non-verifiable.

Histogram binning (HB) was also exploited by [5] for post-hoc calibration. The reported calibration performance was much worse than scaling methods, and it additionally suffered from severe accuracy loss; nonetheless, HB offers verifiable ECEs [13]. In contrast to scaling methods, it produces discrete prediction probabilities, averting quantization at evaluation, and thus its empirical ECE estimate is constant and irrelevant to the number of evaluation bins in the example of Fig. 1-a). Without bias induced by evaluation quantization, its ECE estimate can converge as the variance vanishes with an increased number of evaluation samples, see Fig. 1-b).

Aiming at verifiable ECE evaluation, we propose a novel binning scheme, I-Max binning, that is an outcome of bin optimization via mutual information (MI) maximization. The ranking performance (and accuracy) of a trained classifier depends on how well the ground truth label can be retrieved from the classifier’s output logits. However, binning these logits inherently suffers from information loss. By design, I-Max binning aims to maximally retain the label information given the available number of bins, and also allows the two design objectives, calibration and accuracy, to be nicely disentangled. We evaluate two common variants of HB, i.e., Equal (Eq.) size (uniformly partitioning the probability interval  $[0, 1]$ ) and Eq. mass (uniformly distributing training samples over bins) binning, and explain their accuracy loss through sub-optimal performance at label-information preservation. To cope with a limited number of calibration samples, we propose a novel, sample-efficient strategy that fits one binning scheme for all per-class calibrations, which we call shared class-wise (sCW) I-Max binning.

I-Max binning is evaluated according to multiple performance metrics, including accuracy, ECE (class-wise and top-1 prediction), negative log-likelihood, and Brier score, and compared with benchmark calibration methods across multiple datasets and trained classifiers.

Compared to the baseline, I-Max obtains up to a 38.27% (49.78%) reduction in class-wise ECE and 66.11% (76.07%) reduction in top1-ECE for ImageNet (CIFAR100). Similarly, compared to the state-of-the-art scaling method GP [26] and using its evaluation framework, we obtain a 38.14% (47.96%) reduction in class-wise ECE and 34.96% (50.00%) reduction in top1-ECE for ImageNet (CIFAR100). We additionally extend our sCW calibration idea to other calibration methods, as well as combine I-Max binning with scaling methods for further improved performance.

## 2 Related Work

Confidence calibration is an active research topic in deep learning. Bayesian DNNs [2, 9, 16] and their approximations [4, 15] are resource-demanding methods which consider predictive model uncertainty. However, applications with limited complexity overhead and latency require sampling-free and single-model based calibration methods. Examples include modifying the training loss [14], scalable Gaussian processes [18], sampling-free uncertainty estimation [22], data augmentation [20, 25, 28, 7] and ensemble distribution distillation [17]. In comparison, a simple approach that requires no retraining of the models is post-hoc calibration [5].

Prediction probabilities (logits) scaling and binning are the two main solutions for post-hoc calibration. Scaling methods use parametric or non-parametric models to adjust the raw logits. [5] investigated linear models, ranging from the single-parameter based temperature scaling to more complicated vector/matrix scaling. To avoid overfitting, [12] suggested to regularize matrix scaling with a  $L_2$  loss on the model weights. Recently, [26] adopted a latent Gaussian process for multi-class calibration.

As an alternative to scaling, HB quantizes the raw confidences with either Eq. size or Eq. mass bins [29]. Isotonic regression [30] and Bayesian binning into quantiles (BBQ) [19] are often viewed as binning methods. However, from the verifiable ECE viewpoint, they are scaling methods: though isotonic regression fits a piecewise linear function, its predictions are continuous as they are interpolated for unseen data. BBQ considers multiple binning schemes with different numbers of bins, and combines them using a continuous Bayesian score, resulting in continuous predictions.

Based on empirical results [5] concluded that HB underperforms compared to scaling. However, one critical issue of scaling methods discovered in the recent work [13] is their non-verifiable ECE under sample-based evaluation. As HB offers verifiable ECE evaluation, [13] proposed to apply it after scaling. In this work, we improve the current HB design by casting bin optimization into a MI maximization problem. The resulting I-Max binning is superior to existing scaling methods on multiple evaluation criteria. Furthermore, our findings can also be used to improve scaling methods.

### 3 Method

Here we introduce the I-Max binning scheme, which addresses the issues of HB in terms of preserving label-information in multi-class calibration. After the problem setup in Sec. 3.1, Sec. 3.2) presents a sample-efficient technique for one-vs-rest calibration. In Sec. 3.3 we formulate the training objective of binning as MI maximization and derive a simple algorithm for I-Max binning.

#### 3.1 Problem Setup

We address supervised multi-class classification tasks, where each input  $\mathbf{x} \in \mathcal{X}$  belongs to one of  $K$  classes, and the ground truth labels are one-hot encoded, i.e.,  $\mathbf{y} = [y_1, y_2, \dots, y_K] \in \{0, 1\}^K$ . Let  $f : \mathcal{X} \mapsto \mathbb{R}^K$  be a DNN trained using cross-entropy loss.  $f$  maps each  $\mathbf{x}$  onto a logit vector  $\mathbf{z} = [z_1, \dots, z_K] \in \mathbb{R}^K$ , and its softmax responses  $q_k = \text{softmax}_k(\mathbf{z}) = \frac{e^{z_k}}{\sum_{k'} e^{z_{k'}}$ ,  $k = 1, \dots, K$  are used to rank the  $K$  possible classes of the current instance, i.e.,  $\arg \max_k q_k$  being the top-1 ranked class. The ranking performance of  $\{q_k\}$  determines the classifier’s top- $k$  prediction accuracy. Besides ranking,  $\{q_k\}$  are frequently interpreted as an approximation to the ground truth prediction distribution. However, as the trained classifier tends to overfit to the cross-entropy loss rather than the accuracy (i.e., 0/1 loss),  $\{q_k\}$  as prediction probabilities are typically poorly calibrated. ECE averaged over the  $K$  classes quantifies the multi-class calibration performance of  $f$ :

$${}_{\text{cw}}\text{ECE}(f) = \frac{1}{K} \sum_{k=1}^K E_{\mathbf{z}=f(\mathbf{x})} \left\{ \left| p(y_k = 1 | q_k(\mathbf{z})) - q_k(\mathbf{z}) \right| \right\}. \quad (1)$$

It measures the expected deviation of the ground truth probability  $p(y_k = 1 | q_k(\mathbf{z}))$  from the predicted per-class confidence  $q_k$ . Multi-class post-hoc calibration uses a calibration set  $\mathcal{C}$ , independent from the classifier training set, in order to reduce  ${}_{\text{cw}}\text{ECE}$  by revising  $q_k(\mathbf{z})$ , e.g. by scaling or binning.

For evaluation, the unknown ground truth  $p(y_k = 1 | q_k(\mathbf{z}))$  is empirically estimated from the labeled samples that receive the same prediction confidence  $q_k$ . Since continuous prediction probabilities are naturally non-repetitive, additional quantization is inevitable for evaluating scaling methods.

#### 3.2 One-vs-Rest Strategy for Multi-class Calibration

Histogram binning (HB) was initially developed for two-class calibration. When dealing with multi-class calibration, it separately calibrates each class in a *one-vs-rest* fashion: For any class- $k$  we use  $y_k$  as the binary label for a two-class calibration task, in which the class-1 means  $y_k = 1$  and class-0 collects all other  $K - 1$  classes. We can use a scalar logit  $\lambda_k = z_k - \log \sum_{k' \neq k} e^{z_{k'}}$  to parameterize

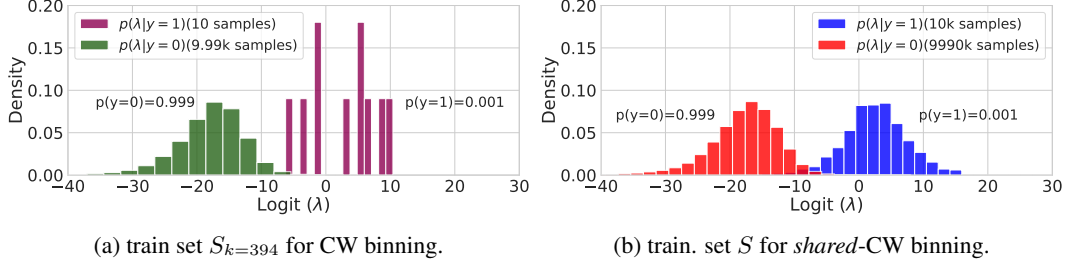


Figure 2: Histogram of ImageNet (InceptionResNetv2) logits for (a) CW and (b) sCW training. By means of the set merging strategy to handle the class imbalance 1 : 999,  $S$  has  $K=1000$  times more class-1 samples than  $S_k$  with the same 10k calibration samples from  $C$ .

the raw prediction probability of  $y_k \in \{0, 1\}$  using the sigmoid-model, i.e.,  $\sigma[\cdot]$

$$P_\sigma(y_k; \lambda_k) = \sigma[(2y_k - 1)\lambda_k] = \begin{cases} q_k & y_k = 1; \\ 1 - q_k & y_k = 0. \end{cases} \quad (2)$$

HB then revises  $q_k(\mathbf{z})$  by mapping the raw logit  $\lambda_k(\mathbf{z})$  onto a given number of bins, and reproducing them with the empirical frequency of class-1 samples in each bin. The empirical frequencies are estimated from the class- $k$  training set  $S_k = \{(y_k, \lambda_k)\}$  that is constructed from the calibration set  $C = \{(y, \mathbf{z})\}$  under the one-vs-rest strategy.

It is important to note that the two-class ratio in  $S_k$  is 1 :  $(K - 1)$ , so  $S_k$  can suffer from a severe class imbalance when  $K$  is large. For ImageNet with 1k classes,  $S_k$  constructed from a class-balanced  $C$  of size 10k contains only  $10k/K = 10$  class-1 samples, see Fig. 2-a). Too few class-1 samples will compromise the optimization of the calibration schemes. To address this, we propose to merge  $\{S_k\}$  across  $K$  classes, i.e.,  $S = \cup_k S_k = \{(y, \lambda)\}$ . The size of the resulting merged set  $S$  will be  $10k \times K = 10m$  and will contain 10k class-1 samples ( $K$  times larger than  $S_k$ ), see Fig. 2-b).

For bin optimization, both  $S_k$  and  $S$  serve as empirical approximations to the inaccessible ground truth distribution  $p(y_k, \lambda_k)$ . The former suffers from high variances, arising from insufficient samples, while the latter is biased due to having samples drawn from the other classes. As the calibration set size is usually small, the variance is expected to outweigh the approximation error over the bias (see an empirical analysis in the appendix). Given that, we propose to use  $S$  for training, yielding one binning scheme shareable to all two-class calibration tasks, i.e., *shared* class-wise (sCW) binning instead of CW binning respectively trained on  $S_k$ .

### 3.3 Bin Optimization via Mutual Information (MI) Maximization

Binning can be viewed as a quantizer  $Q$  that maps the real-valued logit  $\lambda \in \mathbb{R}$  to the bin interval  $m \in \{1, \dots, M\}$  if  $\lambda \in \mathcal{I}_m = [g_{m-1}, g_m)$ , where  $M$  is the total number of bin intervals, and the bin edges  $g_m$  are sorted ( $g_{m-1} < g_m$ , and  $g_0 = -\infty, g_M = \infty$ ). Any logit binned to  $\mathcal{I}_m$  will be reproduced to the same bin representative  $r_m$ . In the context of calibration, the bin representative  $r_m$  assigned to the logit  $\lambda_k$  is used as the calibrated prediction probability of the class- $k$ . As multiple classes can be assigned with the same bin representative, we will then encounter ties when making top- $k$  predictions based on calibrated probabilities. Therefore, binning as lossy quantization generally does not preserve the raw logit-based ranking performance, being subject to potential accuracy loss.

Unfortunately, increasing  $M$  to reduce the quantization error is not a good solution here. For a given calibration set, the number of samples per bin generally reduces as  $M$  increases, and a reliable frequency estimation for setting the bin representatives  $\{r_m\}$  demands sufficient samples per bin.

Considering that the top- $k$  accuracy is an indicator of how well the ground truth label can be recovered from the logits, we propose bin optimization via maximizing the MI between the quantized logits  $Q(\lambda)$  and the label  $y$

$$\{g_m^*\} = \arg \max_{Q: \{g_m\}} I(y; m = Q(\lambda)) \stackrel{(a)}{=} \arg \max_{Q: \{g_m\}} H(m) - H(m|y) \quad (3)$$

where the index  $m$  is viewed as a discrete random variable with  $P(m|y) = \int_{g_{m-1}}^{g_m} p(\lambda|y)d\lambda$  and  $P(m) = \int_{g_{m-1}}^{g_m} p(\lambda)d\lambda$ . Such a formulation offers a quantizer  $Q^*$  optimal at preserving the label

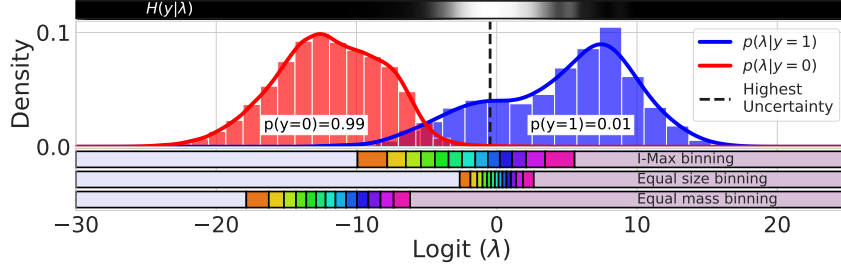


Figure 3: Histogram and KDE of CIFAR100 (WRN) logits in  $S$  constructed from 1k calibration samples. The bin edges of Eq. mass binning are located at the high mass region, mainly covering class-0 due to the imbalanced two class ratio 1 : 99. Both Eq. size and I-Max binning cover the high uncertainty region, but here only I-Max yields reasonable bin widths ensuring enough mass per bin.

information for a given budget on the number of bins. Unlike designing distortion-based quantizers, the reproducer values of raw logits, i.e., the bin representatives  $\{r_m\}$ , are not a part of the optimization space, as it is sufficient to know the mapped bin index of each logit for preserving the label information. In other words, the bin edge and representative settings are disentangled in the MI maximization formulation: the former for preserving label information, and the latter for calibration.

It is interesting to note the equality (a) in (S1), which is based on the relation of MI to the entropy  $H(m)$  and conditional entropy  $H(m|y)$  of  $m$ . Specifically, the first term  $H(m)$  is maximized if  $P(m)$  is uniform, which is attained by Eq. mass binning. As a uniform sample distribution over the bins ensures a balanced empirical frequency estimation quality, it is a desirable choice for setting the bin representatives. However, for MI maximization, equally distributing the mass is insufficient due to the second term  $H(m|y)$ . More importantly, each bin interval should collect the  $\lambda$  that actually encodes the label information, otherwise  $H(m|y)$  will reduce to the entropy  $H(m)$ , and the MI will be zero. As a result, we observe from Fig. 3 that the bin edges of I-Max binning are densely located in an area where the uncertainty of  $y$  given the logit is high. This uncertainty results from small gaps between the top class predictions. With small bin widths, such nearby prediction logits are more likely located to different bins, and thus distinguishable after binning. On the other hand, Eq. mass binning has a single bin stretching across this high-uncertainty area due to the class imbalance (Fig. 3). Eq. size binning follows a pattern closer to I-Max binning.<sup>2</sup> However, its very narrow bin widths around zero may introduce large empirical frequency estimation errors when setting the bin representatives.

For solving the problem (S1), we formulate an equivalent problem.

**Theorem 1.** *The MI maximization problem given in (S1) is equivalent to*

$$\max_{Q:\{g_m\}} I(y; m = Q(\lambda)) \equiv \min_{\{g_m, \phi_m\}} \mathcal{L}(\{g_m, \phi_m\}) \quad (4)$$

where the loss  $\mathcal{L}(\{g_m, \phi_m\})$  is defined as

$$\mathcal{L}(\{g_m, \phi_m\}) \triangleq \sum_{m=0}^{M-1} \int_{g_m}^{g_{m+1}} p(\lambda) \sum_{y' \in \{0,1\}} P(y = y' | \lambda) \log \frac{P(y = y')}{P_\sigma(y = y'; \phi_m)} d\lambda \quad (5)$$

and  $\{\phi_m\}$  as a set of real-valued auxiliary variables are introduced here to ease the optimization.

**Proof.** See the appendix for the proof.  $\square$

Next, we compute the derivatives of the loss  $\mathcal{L}$  with respect to  $\{g_m, \phi_m\}$ . When the conditional distribution  $P(y|\lambda)$  takes the sigmoid model, i.e.,  $P(y|\lambda) \approx \sigma[(2y - 1)\lambda]$ , the stationary points of  $\mathcal{L}$ , zeroing the gradients over  $\{g_m, \phi_m\}$ , have a closed-form expression

$$g_m = \log \left\{ \frac{\log \left[ \frac{1+e^{\phi_m}}{1+e^{-\phi_m-1}} \right]}{\log \left[ \frac{1+e^{-\phi_m-1}}{1+e^{-\phi_m}} \right]} \right\}, \quad \phi_m = \log \left\{ \frac{\int_{g_m}^{g_{m+1}} \sigma(\lambda) p(\lambda) d\lambda}{\int_{g_m}^{g_{m+1}} \sigma(-\lambda) p(\lambda) d\lambda} \right\} \approx \log \left\{ \frac{\sum_{\lambda_n \in S_m} \sigma(\lambda_n)}{\sum_{\lambda_n \in S_m} \sigma(-\lambda_n)} \right\}, \quad (6)$$

<sup>2</sup>Eq. size binning uniformly partitions the interval  $[0, 1]$  in the probability domain. The observed dense and symmetric bin location around zero is the outcome of probability-to-logit translation via the sigmoid function.

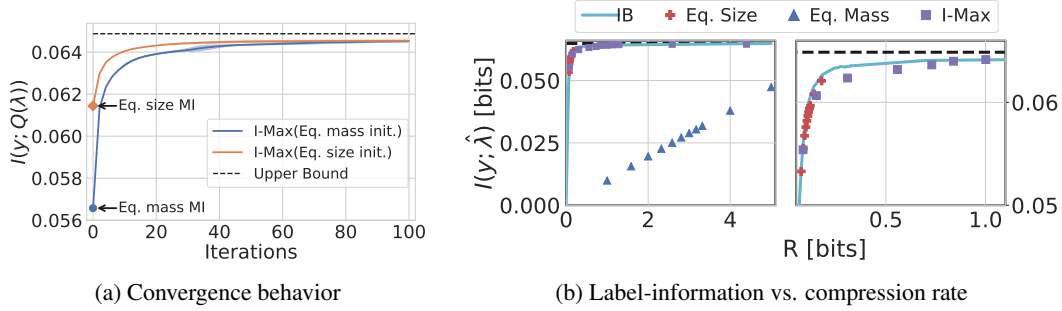


Figure 4: MI evaluation: The KDEs of  $p(\lambda|y)$  for  $y \in \{0, 1\}$  shown in Fig. 3 are used as the ground truth distribution to synthesize a dataset  $S_{\text{kde}}$  and evaluate the MI of Eq. mass, Eq. size, and I-Max binning trained over  $S_{\text{kde}}$ . (a) The developed iterative solution for I-Max bin optimization over  $S_{\text{kde}}$  successfully increases the MI over iterations, approaching the theoretical upper bound  $I(y; \lambda)$ . For comparison, I-Max is initialized with both Eq. size and Eq. mass bin edges, both of which are suboptimal at label information preservation. (b) We compare the three binning schemes with 2 to 16 quantization levels against the information bottleneck (IB) limit on the label-information  $I(y; Q(\lambda))$  vs. the compression rate  $R = I(\lambda; Q(\lambda))$ . The information-rate pairs achieved by I-Max binning are very close to the limit. The information loss of Eq. mass binning is considerably larger, whereas Eq. size binning gets stuck in the low rate regime, failing to reach the upper bound even with more bins.

where the approximation for  $\phi_m$  arises from using the logits in the training set  $S$  as an empirical approximation to  $p(\lambda)$  and  $S_m \triangleq S \cap [g_m, g_{m+1})$ . So, we can solve the problem by iteratively and alternately updating  $\{g_m\}$  and  $\{\phi_m\}$  based on (S12). The convergence and initialization of such an iterative method as well as the sigmoid-model assumption are discussed along with the proof of Theorem 1 in the appendix.

As the iterative method operates under an approximation of the inaccessible ground truth distribution  $p(y, \lambda)$ , here we synthesize an example, see Fig. 4, to assess its effectiveness.<sup>3</sup> In Fig. 4-a, we show the monotonic increase in MI over the iterative steps. Furthermore, Fig. 4-b shows that I-Max approaches the theoretical limits and provides an information-theoretic perspective on the sub-optimal performance of the alternative binning schemes.

## 4 Experiment

**Datasets and Models** We evaluate post-hoc calibration methods on three benchmark datasets, i.e., ImageNet [3], CIFAR-100 [10], and CIFAR-10 [10], and across three modern DNNs for each dataset, i.e., InceptionResNetV2 [24], DenseNet161 [8] and ResNet152 [6] for ImageNet, and Wide ResNet (WRN) [31], DenseNet-BC (L=190, k=40) [8] and ResNext8x64 [27] for the two CIFAR datasets. These models are publicly available pre-trained networks and details are reported in the appendix.

**Training and Evaluation Details** We perform class-balanced random splits of the data test set: the calibration and evaluation set sizes are both 25k for ImageNet, and 5k for the CIFAR datasets. All reported numbers are the means across 5 random splits; stds can be found in the appendix. Note that some calibration methods only use a subset of the available calibration samples for training, showing their sample efficiency. Further calibrator training details are provided in the appendix.

We empirically evaluate MI, Accuracy (top-1 and 5 ACCs), ECE (class-wise and top-1 prediction), NLL and Brier score; the latter is shown in the appendix. The ECEs of the scaling methods are obtained by using Eq. size binning with 100 evaluation bins, as in [26]. Additional quantization schemes for ECE evaluation of *scaling methods* can be found in the appendix.

<sup>3</sup>The formulation (S1) is a special case of IB, i.e., the Lagrange multiplier  $\beta \rightarrow \infty$  and stochastic quantization degenerating to a deterministic one. If using stochastic binning for calibration, it outputs a weighted sum of all bin representatives, thereby being continuous and not ECE verifiable. Given that, we do not use it for calibration.

Table 1: ACCs and ECEs of Eq. mass, Eq. size and I-Max binning for the case of ImageNet (InceptionResNetV2). Due to the poor accuracy of Eq. mass binning, its ECEs are not considered for comparison. The MI is empirically evaluated based on KDE analogous to Fig. 4, where the MI upper bound is  $I(y; \lambda)=0.0068$ . For the other datasets and models, we refer to the appendix.

Binn.	sCW(?)	size	MI $\uparrow$	Acc <sub>top1</sub> $\uparrow$	Acc <sub>top5</sub> $\uparrow$	cwECE $\downarrow$	cwECE <sub><math>\frac{1}{K}</math></sub> $\downarrow$	top1ECE $\downarrow$	NLL $\downarrow$
Baseline	$\times$	-	-	<b>80.33</b>	<b>95.10</b>	0.000442	0.0486	0.0357	0.8406
Eq. Mass	$\times$	25k	0.0026	7.78	27.92	0.000173	0.0016	0.0606	3.5960
	$\checkmark$	1k	0.0026	5.02	26.75	0.000165	0.0022	0.0353	3.5272
Eq. Size	$\times$	25k	0.0053	78.52	89.06	0.000310	0.1344	0.0547	1.5159
	$\checkmark$	1k	0.0062	80.14	88.99	0.000298	0.1525	0.0279	1.2671
I-Max	$\times$	25k	<b>0.0066</b>	80.27	95.01	0.000346	0.0342	0.0329	0.8499
	$\checkmark$	1k	<b>0.0066</b>	80.20	94.86	<b>0.000296</b>	<b>0.0302</b>	<b>0.0200</b>	<b>0.7860</b>

#### 4.1 Eq. Size, Eq. Mass vs. I-Max Binning

When comparing different calibration methods, it is important to jointly consider ECE and ACC. A naive classifier that always predicts all classes with confidence  $1/K$  minimizes the ECE to zero, but its ACC is only at chance level. Additionally, only having a small cwECE may be an artifact. For instance, the cwECE of ImageNet will be dominated by cases where a properly trained classifier ranks the class- $k$  as very unlikely, as the prior ensures the correctness in 99.9% cases. However, in practice, the relevance of the prediction probability being calibrated or not only matters when the event is likely to happen. Given that, we introduce a threshold into the cwECE evaluation as in (1) to only consider cases when the predicted probability of class- $k$  exceeds its prior  $1/K$ .

In Tab. 1, we compare three binning schemes: Eq. size, Eq. mass and I-Max binning. The accuracy performances of the three binning schemes are proportional to their MI (in nats); Eq. mass binning is highly sub-optimal at label information preservation, and thus shows a severe accuracy drop. Eq. size binning accuracy is more similar to that of I-Max binning, but still lower, in particular at Acc<sub>top5</sub>. Also note that I-Max can approach the MI theoretical limit of  $I(y; \lambda)=0.0068$ . Advantages of I-Max become even more prominent when comparing the NLLs of the binning schemes. For all three ECE evaluation metrics, I-Max binning improves on the baseline calibration performance, and outperforms Eq. size binning. Eq. mass binning is out of this comparison scope due to its poor accuracy deeming the method impractical. Overall, I-Max successfully mitigates the negative impact of quantization on ACCs while still providing an improved and verifiable ECE performance. Additionally, I-Max achieves an even better calibration when using sCW with 1k calibration samples, instead of the standard CW binning with 25k calibration samples, highlighting the effectiveness of sCW binning.

In the appendix we perform additional ablations on the number of bins and calibration samples. Accordingly, a post-hoc analysis investigates how the quantization error of the binning schemes change the ranking order. Observations are consistent with the intuition behind the problem formulation (see Sec. 3.3) and empirical results from Tab. 1 that MI maximization is a proper criterion for multi-class calibration and it maximally mitigates the potential accuracy loss.

#### 4.2 Scaling vs. I-Max Binning

In Tab. 2, we compare I-Max binning to benchmark scaling methods. Namely, matrix scaling [12] has a large model capacity compared to other scaling methods using parametric models, while TS [5] only uses a single parameter. As a non-parametric method, GP [26] yields state of the art calibration performance. Benefiting from its model capacity, matrix scaling achieves the best accuracy. I-Max binning achieves the best calibration on CIFAR-100; on ImageNet, it has the best cwECE, and is similar to GP on top1ECE. For a broader scope of comparison, we refer to appendix.

To showcase the complementary nature of scaling and binning, we investigate combining binning with GP (a top performing non-parametric scaling method, though with the drawback of high complexity) and TS (a commonly used scaling method). Here, we propose to bin the raw logits and use the GP/TS scaled logits of the samples per bin for setting the bin representatives, replacing the empirical frequency estimates. As GP is then only needed at the calibration learning phase, complexity is no

Table 2: ACCs and ECEs of I-Max binning (15 bins) and scaling methods. All methods use 1k calibration samples, except for Mtx. Scal., which requires the complete calibration set, i.e., 25k/5k for ImageNet/CIFAR100. Additional 6 scaling methods can be found in the appendix.

Calibrator	CIFAR100 (WRN)			ImageNet (InceptionResNetV2)			
	Acc <sub>top1</sub> ↑	cwECE <sub><math>\frac{1}{K}</math></sub> ↓	top1 ECE ↓	Acc <sub>top1</sub> ↑	Acc <sub>top5</sub> ↑	cwECE <sub><math>\frac{1}{K}</math></sub> ↓	top1 ECE ↓
Baseline	81.35	0.1113	0.0748	80.33	95.10	0.0486	0.0357
Mtx Scal. [12]	<b>81.44</b>	0.1085	0.0692	<b>80.78</b>	<b>95.38</b>	0.0508	0.0282
TS [5]	81.35	0.0911	0.0511	80.33	95.10	0.0559	0.0439
GP [26]	81.34	0.1074	0.0358	80.33	95.11	0.0485	0.0186
I-Max	81.30	0.0518	0.0231	80.20	94.86	0.0302	0.0200
I-Max w. TS	81.34	<b>0.0510</b>	0.0365	80.20	94.87	0.0354	0.0402
I-Max w. GP	81.34	0.0559	<b>0.0179</b>	80.20	94.87	<b>0.0300</b>	<b>0.0121</b>

Table 3: ACCs and ECEs of scaling methods using the one-vs-rest conversion for multi-class calibration. Here we compare using 1k samples for both CW and sCW scaling for ImageNet and CIFAR100. For each scheme and metric, we display the best variant of the scaling methods in bold.

Calibrator	sCW(?)	CIFAR100 (WRN)			ImageNet (InceptionResNetV2)			
		Acc <sub>top1</sub> ↑	cwECE <sub><math>\frac{1}{K}</math></sub> ↓	top1 ECE ↓	Acc <sub>top1</sub> ↑	Acc <sub>top5</sub> ↑	cwECE <sub><math>\frac{1}{K}</math></sub> ↓	top1 ECE ↓
Baseline	-	81.35	0.1113	0.0748	80.33	95.10	0.0489	0.0357
Beta [11]	✗	81.02	0.1066	0.0638	77.80	86.83	0.1662	0.1586
Beta	✓	<b>81.35</b>	0.0942	0.0357	<b>80.33</b>	<b>95.10</b>	0.0625	0.0603
I-Max w. Beta	✓	81.34	<b>0.0508</b>	<b>0.0161</b>	80.20	94.87	<b>0.0381</b>	<b>0.0574</b>
Isotonic Reg. [30]	✗	80.62	0.0989	0.0785	77.82	88.36	0.1640	0.1255
Isotonic Reg.	✓	81.30	0.0602	0.0257	<b>80.22</b>	<b>95.05</b>	0.0345	0.0209
I-Max w. Isotonic Reg.	✓	<b>81.34</b>	<b>0.0515</b>	<b>0.0212</b>	80.20	94.87	<b>0.0299</b>	<b>0.0170</b>
Platt Scal. [21]	✗	81.31	0.0923	0.1035	<b>80.36</b>	94.91	0.0451	0.0961
Platt Scal.	✓	<b>81.35</b>	0.0816	0.0462	80.33	<b>95.10</b>	0.0565	0.0415
I-Max w. Platt Scal.	✓	81.34	<b>0.0511</b>	<b>0.0323</b>	80.20	94.87	<b>0.0293</b>	<b>0.0392</b>

longer an issue. More importantly, binning offers GP/TS (and any scaling method) verifiable ECE performance. Being mutually beneficial, GP helps improving ACCs and ECEs of binning.

Using the combination of the best binning method and scaling method (i.e. I-Max (sCW) w. GP), only marginally degrades the accuracy performance of the baseline by as little as 0.16% (0.012%) on Acc<sub>top1</sub> for ImageNet (CIFAR100) and 0.24% on Acc<sub>top5</sub> for ImageNet. This minor drop is insignificant compared to the improvement in calibration. We obtain a 38.27% (49.78%) reduction in cwECE <sub>$\frac{1}{K}$</sub>  and 66.11% (76.07%) reduction in top1 ECE of the baseline for ImageNet (CIFAR100). Similarly, compared to the state-of-the-art scaling method (i.e. GP [26]), we obtain a 38.14% (47.96%) reduction in top1 ECE and 34.96% (50.00%) reduction in top1-ECE for ImageNet (CIFAR100).

### 4.3 Shared Class Wise Helps Scaling Methods

Though without quantization loss, some scaling methods, i.e., Beta [11], Isotonic regression [30], and Platt scaling [21], even suffer from more severe accuracy degradation than I-Max binning. As they also use the one-vs-rest strategy for multi-class calibration, we find that the proposed shared CW binning strategy is beneficial for reducing their accuracy loss and improving their ECE performance, with only 1k calibration samples, see Tab. 3.

## 5 Conclusion

In this work, we proposed I-Max binning for multi-class calibration. By maximally preserving the label-information under lossy quantization, it outperforms histogram binning (HB) in reducing potential accuracy losses. Additionally, through the novel shared class-wise (sCW) strategy, we solved the sample-inefficiency issue of training binning and scaling methods that rely on one-vs-rest

conversion for multi-class calibration. Our experiments showed that I-Max binning yields consistent class-wise and top-1 calibration improvements over multiple datasets and model architectures, outperforming HB and state-of-the-art scaling methods. The combination of I-Max and scaling methods offers further, and more importantly, verifiable calibration performance gains.

Future work includes diversifying the calibration set through data augmentation or multiple-inference models for generalization to dataset shifts unobserved during training. Another exciting primary direction is the inclusion of I-Max during the classifier’s training, allowing I-Max to influence the logit distribution to exploit further calibration gains. Last but not least, as a quantization scheme, I-Max binning may also be exploited for calibration evaluation, providing better, ideally verifiable empirical ECE estimates of scaling methods.

## References

- [1] David Arthur and Sergei Vassilvitskii. k-means++: the advantages of careful seeding. In *Proceedings of the ACM-SIAM symposium on Discrete algorithms*, pp. 1027–1035, Philadelphia, PA, USA, 2007.
- [2] Charles Blundell, Julien Cornebise, Koray Kavukcuoglu, and Daan Wierstra. Weight uncertainty in neural networks. In *International Conference on Machine Learning (ICML)*, pp. 1613–1622, Lille, France, July 2015.
- [3] J. Deng, W. Dong, R. Socher, L.-J. Li, K. Li, and L. Fei-Fei. ImageNet: A Large-Scale Hierarchical Image Database. In *Proc. of the IEEE/CVF Int. Conf. on Computer Vision and Pattern Recognition (CVPR)*, 2009.
- [4] Yarın Gal and Zoubin Ghahramani. Dropout as a bayesian approximation: Representing model uncertainty in deep learning. In *International Conference on Machine Learning (ICML)*, 2016.
- [5] Chuan Guo, Geoff Pleiss, Yu Sun, and Kilian Q. Weinberger. On calibration of modern neural networks. In *International Conference on Machine Learning (ICML)*, pp. 1321–1330, Sydney, Australia, August 2017.
- [6] Kaiming He, Xiangyu Zhang, Shaoqing Ren, and Jian Sun. Deep residual learning for image recognition. *2016 IEEE Conference on Computer Vision and Pattern Recognition (CVPR)*, pp. 770–778, 2016.
- [7] Dan Hendrycks, Norman Mu, Ekin Dogus Cubuk, Barret Zoph, Justin Gilmer, and Balaji Lakshminarayanan. Augmix: A simple method to improve robustness and uncertainty under data shift. In *International Conference on Learning Representations (ICLR)*, 2020.
- [8] G. Huang, Z. Liu, L. v. d. Maaten, and K. Q. Weinberger. Densely connected convolutional networks. In *Proc. of the IEEE Conference on Computer Vision and Pattern Recognition (CVPR)*, 2017.
- [9] Durk P Kingma, Tim Salimans, and Max Welling. Variational dropout and the local reparameterization trick. In *Advances in Neural Information Processing Systems (NeurIPS)*, pp. 2575–2583, 2015.
- [10] Alex Krizhevsky. Learning multiple layers of features from tiny images. Technical report, 2009.
- [11] Meelis Kull, Telmo Silva Filho, and Peter Flach. Beta calibration: a well-founded and easily implemented improvement on logistic calibration for binary classifiers. In *International Conference on Artificial Intelligence and Statistics (AISTATS)*, pp. 623–631, Fort Lauderdale, FL, USA, April 2017.
- [12] Meelis Kull, Miquel Perello Nieto, Markus Kängsepp, Telmo Silva Filho, Hao Song, and Peter Flach. Beyond temperature scaling: Obtaining well-calibrated multi-class probabilities with dirichlet calibration. In *Advances in Neural Information Processing Systems (NeurIPS)*, pp. 12295–12305, 2019.
- [13] Ananya Kumar, Percy S Liang, and Tengyu Ma. Verified uncertainty calibration. In *Advances in Neural Information Processing Systems (NeurIPS)*, pp. 3787–3798, 2019.
- [14] Aviral Kumar, Sunita Sarawagi, and Ujjwal Jain. Trainable calibration measures for neural networks from kernel mean embeddings. In *International Conference on Machine Learning (ICML)*, pp. 2805–2814, July 2018.
- [15] Balaji Lakshminarayanan, Alexander Pritzel, and Charles Blundell. Simple and scalable predictive uncertainty estimation using deep ensembles. In *Advances in Neural Information Processing Systems (NeurIPS)*. 2017.
- [16] Christos Louizos and Max Welling. Multiplicative normalizing flows for variational Bayesian neural networks. In *International Conference on Machine Learning (ICML)*, pp. 2218–2227, Sydney, Australia, August 2017.

- [17] Andrey Malinin, Bruno Mlodozienec, and Mark Gales. Ensemble distribution distillation. In *International Conference on Learning Representations (ICLR)*, 2020.
- [18] Dimitrios Miliotis, Raffaello Camoriano, Pietro Michiardi, Lorenzo Rosasco, and Maurizio Filippone. Dirichlet-based gaussian processes for large-scale calibrated classification. In S. Bengio, H. Wallach, H. Larochelle, K. Grauman, N. Cesa-Bianchi, and R. Garnett (eds.), *Advances in Neural Information Processing Systems (NeurIPs)*, pp. 6005–6015, 2018.
- [19] Mahdi Pakdaman Naeini, Gregory F. Cooper, and Milos Hauskrecht. Obtaining well calibrated probabilities using Bayesian binning. In *Proc. of Conference on Artificial Intelligence (AAAI)*, pp. 2901–2907, 2015.
- [20] Kanil Patel, William Beluch, Dan Zhang, Michael Pfeiffer, and Bin Yang. On-manifold adversarial data augmentation improves uncertainty calibration. *arXiv*, 2019.
- [21] John Platt. Probabilities for SV machines. In *Advances in Large Margin Classifiers*, pp. 61–74, 01 1999.
- [22] Janis Postels, Francesco Ferroni, Huseyin Coskun, Nassir Navab, and Federico Tombari. Sampling-free epistemic uncertainty estimation using approximated variance propagation. In *Proc. of the IEEE International Conference on Computer Vision (ICCV)*, October 2019.
- [23] Serim Ryou, Seong-Gyun Jeong, and Pietro Perona. Anchor loss: Modulating loss scale based on prediction difficulty. In *Proc. of the IEEE International Conference on Computer Vision (ICCV)*, October 2019.
- [24] Christian Szegedy, Sergey Ioffe, Vincent Vanhoucke, and Alexander A. Alemi. Inception-v4, Inception-ResNet and the impact of residual connections on learning. In *Proc. of the Conference on Artificial Intelligence*, pp. 4278–4284, San Francisco, U.S., February 2017.
- [25] Sunil Thulasidasan, Gopinath Chennupati, Jeff Bilmes, Tanmoy Bhattacharya, and Sarah Michalak. On mixup training: Improved calibration and predictive uncertainty for deep neural networks. *Advances in Neural Information Processing Systems (NeurIPs)*, 2019.
- [26] Jonathan Wenger, Hedvig Kjellström, and Rudolph Triebel. Non-parametric calibration for classification. In *International Conference on Artificial Intelligence and Statistics (AISTATS)*, 2020.
- [27] Saining Xie, Ross B. Girshick, Piotr Dollár, Zhuowen Tu, and Kaiming He. Aggregated residual transformations for deep neural networks. *Proc. of the IEEE Conference on Computer Vision and Pattern Recognition (CVPR)*, 2017.
- [28] Sangdoon Yun, Dongyoon Han, Seong Joon Oh, Sanghyuk Chun, Junsuk Choe, and Youngjoon Yoo. Cutmix: Regularization strategy to train strong classifiers with localizable features. In *Proc. of the IEEE International Conference on Computer Vision (ICCV)*, 2019.
- [29] Bianca Zadrozny and Charles Elkan. Obtaining calibrated probability estimates from decision trees and naive bayesian classifiers. In *International Conference on Machine Learning (ICML)*, pp. 609–616, 2001.
- [30] Bianca Zadrozny and Charles Elkan. Transforming classifier scores into accurate multiclass probability estimates. In *SIGKDD Conference on Knowledge Discovery and Data Mining*, pp. 694–699, January 2002.
- [31] Sergey Zagoruyko and Nikos Komodakis. Wide residual networks. In *Proceedings of the British Machine Vision Conference (BMVC)*, 2016.

This document supplements the presentation of *Multi-Class Uncertainty Calibration via Mutual Information Maximization-based Binning* in the main paper with the following:

- S1: No extra normalization after  $K$  class-wise calibrations;
- S2:  $S$  vs.  $S_k$  as empirical approximations to  $p(\lambda_k, y_k)$  for bin optimization in Sec. 3.2;
- S3: Mathematical proof for Theorem 1 in Sec. 3.3;
- S4: Post-hoc analysis on the experiment results in Sec. 4.1;
- S5: Ablation on the number of bins and calibration set size;
- S6: Empirical ECE estimation of scaling methods under multiple evaluation schemes;
- S7: Training details;
- S8: Extend Tab. 1 in Sec. 4.1 for more datasets and models;
- S9: Extend Tab. 2 in Sec. 4.2 for more scaling methods, datasets and models.

## S1 No Extra Normalization after $K$ Class-wise Calibrations

There is a group of calibration schemes that rely on one-vs-rest conversion to turn multi-class calibration into  $K$  class-wise calibrations, e.g., histogram binning (HB), Platt scaling and Isotonic regression. After per-class calibration, the calibrated prediction probabilities of all classes no longer fulfill the constraint, i.e.,  $\sum_{k=1}^K q_k \neq 1$ . An extra normalization step was taken in [5] to regain the normalization constraint. Here, we note that this extra normalization is unnecessary and partially undoes the per-class calibration effect. For HB, normalization even renders its ECE evaluation non-verifiable like any other scaling methods.

One-vs-rest strategy essentially marginalizes the multi-class predictive distribution over each class. After such marginalization, each class and its prediction probability shall be treated independently, thus no longer being constrained by the multi-class normalization constraint. This is analogous to train a CIFAR or ImageNet classifier with sigmoid rather than softmax cross entropy loss, e.g., [23]. At training and test time, each class prediction probability is individually taken from the respective sigmoid-response without normalization. The class with the largest response is then top-ranked, and normalization itself has no influence on the ranking performance.

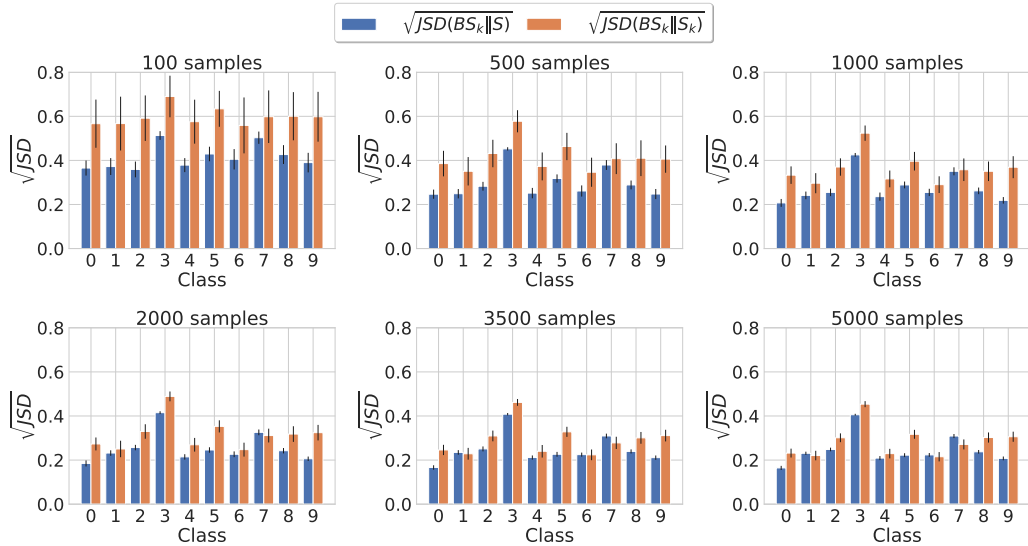


Figure S1: Empirical approximation error of  $S$  vs.  $S_k$ , where Jensen-Shannon divergence (JSD) is used to measure the difference between the empirical distributions underlying the training sets for class-wise bin optimization. Overall, the merged set  $S$  is a more sample efficient choice over  $S_k$ .

## S2 $S$ vs. $S_k$ as Empirical Approximations to $p(\lambda_k, y_k)$ for Bin Optimization

In Sec. 3.2 of the main paper, we discussed the class imbalance issue, arising from one-vs-rest conversion, see Fig. 2. To tackle it, we proposed to merge the class-wise (CW) bin training sets  $\{S_k\}$  and use the merged one  $S$  to train a single binning scheme for all classes, i.e., shared CW (sCW) instead of CW binning. Tab. 3 showed that our proposal is also beneficial to scaling methods that use one-vs-rest for multi-class calibration.

As pointed out in Sec. 3.2, both  $S$  and  $S_k$  are empirical approximations to the inaccessible ground truth  $p(\lambda_k, y_k)$  for bin optimization. In Fig. S1, we empirically analyze their approximation errors. From the CIFAR10 test set, we take 5k samples to approximate per-class logit distribution  $p(\lambda_k|y_k = 1)$  by means of histogram density estimation<sup>4</sup>, and then use it as the baseline for comparison, i.e.,  $BS_k$  in Fig. S1. The rest of the 5k samples in the CIFAR10 test set are reserved for constructing  $S_k$  and  $S$ . For each class, we respectively evaluate the square root of the Jensen-Shannon divergence (JSD) from the baseline  $BS_k$  to the empirical distribution of  $S$  or  $S_k$  attained at different numbers of samples. Despite suffering from the bias induced by set merging,  $S$  achieves noticeably smaller JSDs than  $S_k$  in nearly all cases, and shows to be more sample efficient. Only after using all 5k samples,  $S_k$  has slightly smaller JSDs than  $S$  in the class-1, and 6 and 7. From CIFAR10 to CIFAR100 and ImageNet, the class imbalance issue becomes more severe. We expect the sample inefficiency issue of  $S_k$  becomes more critical, and therefore it is advisable to use  $S$  for bin optimization.

## S3 Proof of Theorem 1

**Theorem 1.** *The mutual information (MI) maximization problem given as follows:*

$$\{g_m^*\} = \arg \max_{Q: \{g_m\}} I(y; m = Q(\lambda)) \quad (S1)$$

is equivalent to

$$\max_{Q: \{g_m\}} I(y; m = Q(\lambda)) \equiv \min_{\{g_m, \phi_m\}} \mathcal{L}(\{g_m, \phi_m\}) \quad (S2)$$

where the loss  $\mathcal{L}(\{g_m, \phi_m\})$  is defined as

$$\mathcal{L}(\{g_m, \phi_m\}) \triangleq \sum_{m=0}^{M-1} \int_{g_m}^{g_{m+1}} p(\lambda) \sum_{y' \in \{0,1\}} P(y = y' | \lambda) \log \frac{P(y = y')}{P_\sigma(y = y'; \phi_m)} d\lambda \quad (S3)$$

$$\text{with } P_\sigma(y; \phi_m) \triangleq \sigma[(2y - 1)\phi_m]. \quad (S4)$$

As a set of real-valued auxiliary variables,  $\{\phi_m\}$  are introduced here to ease the optimization.

**Proof.** Before starting our proof, we note that the upper-case  $P$  indicates probability mass functions of discrete random variables, e.g., the label  $y \in \{0, 1\}$  and the bin interval index  $m \in \{1, \dots, M\}$ ; whereas the lower-case  $p$  is reserved for probability density functions of continuous random variables, e.g., the raw logit  $\lambda \in \mathbb{R}$ .

The key to prove the equivalence is to show the inequality

$$I(y; m = Q(\lambda)) \geq -\mathcal{L}(\{g_m, \phi_m\}), \quad (S5)$$

and the equality is attainable by minimizing  $\mathcal{L}$  over  $\{\phi_m\}$ .

By the definition of MI, we firstly expand  $I(y; m = Q(\lambda))$  as

$$I(y; m = Q(\lambda)) = \sum_{i=0}^{M-1} \int_{g_m}^{g_{m+1}} p(\lambda) \sum_{y' \in \{0,1\}} P(y = y' | \lambda) \log \frac{P(y = y' | m)}{P(y = y')} d\lambda, \quad (S6)$$

where the conditional distribution  $P(y|m)$  is given as

$$P(y|m) = P(y|\lambda \in [g_m, g_{m+1})) = \frac{P(y) \int_{g_m}^{g_{m+1}} p(\lambda|y) d\lambda}{\int_{g_m}^{g_{m+1}} p(\lambda) d\lambda} = \frac{\int_{g_m}^{g_{m+1}} p(y|\lambda) P(y) d\lambda}{\int_{g_m}^{g_{m+1}} p(\lambda) d\lambda}. \quad (S7)$$

<sup>4</sup>Here, we focus on  $p(\lambda_k|y_k = 1)$  as its empirical estimation suffers from the class imbalance, being much more challenging than  $p(\lambda_k|y_k = 0)$  as illustrated in Fig. 2 of the main paper.

From the above expression, we note that MI maximization effectively only accounts to the bin edges  $\{g_m\}$ . The bin representatives can be arbitrary as long as they can indicate the condition  $\lambda \in [g_m, g_{m+1})$ . So, the bin interval index  $m$  is sufficient to serve the role in conditioning the probability mass function of  $y$ , i.e.,  $P(y|m)$ . After optimizing the bin edges, we have the freedom to set the bin representatives for the sake of post-hoc calibration.

Next, based on the MI expression, we compute its sum with  $\mathcal{L}$

$$\begin{aligned}
I(y; Q(\lambda)) + \mathcal{L}(\{g_m, \phi_m\}) &= \sum_{i=0}^{M-1} \int_{g_m}^{g_{m+1}} p(\lambda) \sum_{y' \in \{0,1\}} P(y = y'|\lambda) d\lambda \log \frac{P(y = y'|m)}{P_\sigma(y = y'; \phi_m)} \\
&\stackrel{(a)}{=} \sum_{i=0}^{M-1} P(m) \left[ \sum_{y' \in \{0,1\}} P(y = y'|m) \log \frac{P(y = y'|m)}{P_\sigma(y = y'; \phi_m)} \right] \\
&\stackrel{(b)}{=} \sum_{i=0}^{M-1} P(m) \text{KLD} [P(y = y'|m) \| P_\sigma(y = y'; \phi_m)] \\
&\stackrel{(c)}{\geq} 0. \tag{S8}
\end{aligned}$$

The equality (a) is based on

$$\int_{g_m}^{g_{m+1}} p(\lambda) P(y = y'|\lambda) d\lambda = P(y = y', \lambda \in [g_m, g_{m+1})) = \underbrace{P(\lambda \in [g_m, g_{m+1}))}_{=P(m)} P(y = y'|m). \tag{S9}$$

From the equality (a) to (b), it is simply because of identifying the term in  $[\cdot]$  of the equality (a) as the Kullback-Leibler divergence (KLD) between two probability mass functions of  $y$ . As the probability mass function  $P(m)$  and the KLD both are non-negative, we reach to the inequality at (c), where the equality holds if  $P_\sigma(y; \phi_m) = P(y|m)$ . By further noting that  $\mathcal{L}$  is convex over  $\{\phi_m\}$  and  $P_\sigma(y; \phi_m) = P(y|m)$  nulls out its gradient over  $\{\phi_m\}$ , we then reach to

$$I(y; Q(\lambda)) + \min_{\{\phi_m\}} \mathcal{L}(\{g_m, \phi_m\}) = 0. \tag{S10}$$

The obtained equality then concludes our proof

$$\begin{aligned}
\max_{\{g_m\}} I(y; Q(\lambda)) &= \max_{\{g_m\}} \left[ - \min_{\{\phi_m\}} \mathcal{L}(\{g_m, \phi_m\}) \right] = - \min_{\{g_m, \phi_m\}} \mathcal{L}(\{g_m, \phi_m\}) \\
&\equiv \min_{\{g_m, \phi_m\}} \mathcal{L}(\{g_m, \phi_m\}). \tag{S11}
\end{aligned}$$

□

### S3.1 Convergence of the Iterative Method

For convenience, we recall the update equations for  $\{g_m, \phi_m\}$  in Sec. 3.3 of the main paper here

$$\begin{aligned}
g_m &= \log \left\{ \frac{\log \left[ \frac{1+e^{\phi_m}}{1+e^{\phi_m-1}} \right]}{\log \left[ \frac{1+e^{-\phi_m-1}}{1+e^{-\phi_m}} \right]} \right\} \\
\phi_m &= \log \left\{ \frac{\int_{g_m}^{g_{m+1}} \sigma(\lambda) p(\lambda) d\lambda}{\int_{g_m}^{g_{m+1}} \sigma(-\lambda) p(\lambda) d\lambda} \right\} \approx \log \left\{ \frac{\sum_{\lambda_n \in \mathcal{S}_m} \sigma(\lambda_n)}{\sum_{\lambda_n \in \mathcal{S}_m} \sigma(-\lambda_n)} \right\} \quad \forall m. \tag{S12}
\end{aligned}$$

In the following, we show that the updates on  $\{g_m\}$  and  $\{\phi_m\}$  according to (S12) continuously decrease the loss  $\mathcal{L}$ , i.e.,

$$\mathcal{L}(\{g_m^l, \phi_m^l\}) \geq \mathcal{L}(\{g_m^{l+1}, \phi_m^l\}) \geq \mathcal{L}(\{g_m^{l+1}, \phi_m^{l+1}\}). \tag{S13}$$

The second inequality is based on the explained property of  $\mathcal{L}$ . Namely, it is convex over  $\{\phi_m\}$  and the minimum for any given  $\{g_m\}$  is attained by  $P_\sigma(y; \phi_m) = P(y|m)$ . As  $\phi_m$  is the log-probability ratio of  $P_\sigma(y; \phi_m)$ , we shall have

$$\phi_m^{l+1} \leftarrow \log \frac{P(y = 1|m)}{P(y = 0|m)} \tag{S14}$$

where  $P(y = 1|m)$  in this case is induced by  $\{g_m^{l+1}\}$  and  $P(y|\lambda) = \sigma[(2y - 1)\lambda]$ . Plugging  $\{g_m^{l+1}\}$  and  $P(y|\lambda) = \sigma[(2y - 1)\lambda]$  into (S7), the resulting  $P(y = y'|m)$  at the iteration  $l + 1$  yields the update equation of  $\phi_m$  as given in (S12).

To prove the first inequality, we start from showing that  $\{g_m^{l+1}\}$  is a local minimum of  $\mathcal{L}(\{g_m, \phi_m^l\})$ . The update equation on  $\{g_m\}$  is an outcome of solving the stationary point equation of  $\mathcal{L}(\{g_m, \phi_m^l\})$  over  $\{g_m\}$  under the condition  $p(\lambda = g_m) > 0$  for any  $m$

$$\frac{\partial \mathcal{L}(\{g_m, \phi_m^l\})}{\partial g_m} = p(\lambda = g_m) \sum_{y' \in \{0,1\}} P(y = y'|\lambda = g_m) \log \frac{P_\sigma(y = y'; \phi_m^l)}{P_\sigma(y = y'; \phi_{m-1}^l)} \stackrel{!}{=} 0 \quad \forall m \quad (\text{S15})$$

Being a stationary point is the necessary condition of local extremum when the function's first-order derivative exists at that point, i.e., first-derivative test. To further show that the local extremum is actually a local minimum, we resort to the second-derivative test, i.e., if the Hessian matrix of  $\mathcal{L}(\{g_m, \phi_m^l\})$  is positive definite at the stationary point  $\{g_m^{l+1}\}$ . Due to  $\phi_m > \phi_{m-1}$  with the monotonically increasing function sigmoid in its update equation, we have

$$\frac{\partial^2 \mathcal{L}(\{g_m, \phi_m^l\})}{\partial g_m \partial g_{m'}} \Big|_{g_m = g_m^{l+1} \forall m} = 0 \quad \text{and} \quad \frac{\partial^2 \mathcal{L}(\{g_m, \phi_m^l\})}{\partial^2 g_m} \Big|_{g_m = g_m^{l+1} \forall m} > 0, \quad (\text{S16})$$

implying that all eigenvalues of the Hessian matrix are positive (equivalently, is positive definite). Therefore,  $\{g_m^{l+1}\}$  as the stationary point of  $\mathcal{L}(\{g_m, \phi_m^l\})$  is a local minimum.

It is important to note that from the stationary point equation (S15),  $\{g_m^{l+1}\}$  as a local minimum is unique among  $\{g_m\}$  with  $p(\lambda = g_m) > 0$  for any  $m$ . In other words, the first inequality holds under the condition  $p(\lambda = g_m) > 0$  for any  $m$ . Binning is a lossy data processing. In order to maximally preserve the label information, it is natural to exploit all bins in the optimization, not wasting any single bin in the area without mass, i.e.,  $p(\lambda = g_m) = 0$ . Having said that, it is reasonable to constrain  $\{g_m\}$  with  $p(\lambda = g_m) > 0 \forall m$  over iterations, thereby concluding that the iterative method will converge to a local minimum based on the two inequalities (S13).

### S3.2 Initialization of the Iterative Method

We propose to initialize the iterative method by modifying the k-means++ algorithm [1] that was developed to initialize the cluster centers for k-means clustering algorithms. It is based on the following identification

$$\mathcal{L}(\{g_m, \phi_m\}) + I(y; \lambda) = \sum_{i=0}^{M-1} \int_{g_m}^{g_{m+1}} p(\lambda) \text{KDL} [P(y = y'|\lambda) \| P_\sigma(y = y'; \phi_m)] d\lambda \quad (\text{S17})$$

$$\begin{aligned} &\geq \int_{-\infty}^{\infty} p(\lambda) \min_m \text{KLD} [P(y = y'|\lambda) \| P_\sigma(y = y'; \phi_m)] d\lambda \\ &\approx \frac{1}{|S|} \sum_{\lambda_n \in S} \min_m \text{KLD} [P(y = y'|\lambda_n) \| P_\sigma(y = y'; \phi_m)]. \end{aligned} \quad (\text{S18})$$

As  $I(y; \lambda)$  is a constant with respect to  $(\{g_m, \phi_m\})$ , minimizing  $\mathcal{L}$  is equivalent to minimizing the term on the RHS of (S17). The last approximation is reached by turning the binning problem into a clustering problem, i.e., grouping the logit samples in the training set  $S$  according to the KLD measure, where  $\{\phi_m\}$  are effectively the centers of each cluster. k-means++ algorithm [1] initializes the cluster centers based on the Euclidean distance. In our case, we alternatively use the JSD as the distance measure to initialize  $\{\phi_m\}$ . Comparing with KLD, JSD is symmetric and bounded.

### S3.3 A Remark on the Iterative Method Derivation

The closed-form update on  $\{g_m\}$  in (S12) is based on the sigmoid-model approximation, which has been validated through our empirical experiments. It is expected to work with properly trained classifiers that are not overly overfitting to the cross-entropy loss, e.g., using data augmentation and other regularization techniques at training. Nevertheless, even in corner cases that classifiers are poorly trained, the iterative method can still be operated without the sigmoid-model approximation.

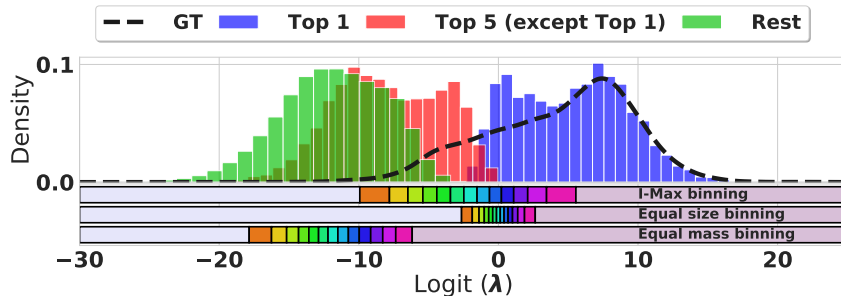


Figure S2: Histogram of CIFAR100 (WRN) logits in  $S$  constructed from 1k calibration samples, using the same setting as Fig. 3 in the main paper. Instead of categorizing the logits according to their two-class label  $y_k \in \{0, 1\}$  as in Fig. 3, here we sort them according to their ranks given by the CIFAR100 WRN classifier. As a baseline, we also plot the KDE of logits associated to the ground truth classes, i.e., GT.

Namely, as shown in Fig. 3 of the main paper, we can resort to KDE for an empirical estimation of the ground truth distribution  $p(\lambda|y)$ . Using the KDEs, we can compute the gradient of  $\mathcal{L}$  over  $\{g_m\}$  and perform iterative gradient based update on  $\{g_m\}$ , replacing the closed-form based update. Essentially, the sigmoid-model approximation is only necessary to find the stationary points of the gradient equations, speeding up the convergence of the method. If attempting to keep the closed-form update on  $\{g_m\}$ , an alternative solution could be to use the KDEs for adjusting the sigmoid-model, e.g.,  $p(y|\lambda) \approx \sigma[(2y-1)(a\lambda+ab)]$ , where  $a$  and  $b$  are chosen to match the KDE based approximation to  $p(y|\lambda)$ . After setting  $a$  and  $b$ , they will be used as a scaling and bias term in the original closed-form update equations

$$g_m = \frac{1}{a} \log \left\{ \frac{\log \left[ \frac{1+e^{\phi_m}}{1+e^{\phi_m-1}} \right]}{\log \left[ \frac{1+e^{-\phi_m}}{1+e^{-\phi_m-1}} \right]} \right\} - b \quad \forall m. \quad (\text{S19})$$

$$\phi_m = \log \left\{ \frac{\int_{g_m}^{g_m+1} \sigma(a\lambda+ab)p(\lambda)d\lambda}{\int_{g_m}^{g_m+1} \sigma(-a\lambda-ab)p(\lambda)d\lambda} \right\} \approx \log \left\{ \frac{\sum_{\lambda_n \in S_m} \sigma(a\lambda_n+ab)}{\sum_{\lambda_n \in S_m} \sigma(-a\lambda_n-ab)} \right\}$$

## S4 Post-hoc Analysis on the Experiment Results in Sec. 4.1

In Tab. 1 of Sec. 4.1, we compared three different binning schemes by measuring their ACCs and ECEs. The observation on their accuracy performance is aligned with our mutual information maximization viewpoint introduced in Sec. 3.3 and Fig. 3. Here, we re-present Fig. 3 and provide an alternative explanation to strengthen our understanding on how the location of bin edges affects the accuracy, e.g., why Eq. Size binning performed acceptable at the top-1 ACC, but failed at the top-5 ACC. Specifically, Fig. S2 shows the histograms of raw logits that are grouped based on their ranks instead of their labels as in Fig. 3. As expected, the logits with low ranks (i.e., rest below top-5 in Fig. S2) are small and thus take the left hand side of the plot, whereas the top-1 logits are mostly located on the right hand side. Besides sorting logits according to their ranks, we additionally estimate the density of the ground truth (GT) classes associated logits, i.e., GT in Fig. S2). With a properly trained classifier, the histogram of top-1 logits shall largely overlap with the density curve GT, i.e., top-1 prediction being correct in most cases.

From the bin edge location of Eq. Mass binning, it attempts to attain small quantization errors for logits of low ranks rather than top-5. This will certainly degrade the accuracy performance after binning. On contrary, Eq. Size binning aims at small quantization error for the top-1 logits, but ignores top-5 ones. As a result, we observed its poor top-5 ACCs. I-Max binning nicely distributes its bin edges in the area where the GT logits are likely to locate, and the bin width becomes smaller in the area where the top-5 logits are close by (i.e., the overlap region between the red and blue histograms). Note that, any logit larger than zero must be top-1 ranked, as there can exist at most one class with prediction probability larger than 0.5. Given that, the bins located above zero are no longer to maintain the ranking order, rather to reduce the precision loss of top-1 prediction probability after binning.

Table S1: Comparison of sCW binning methods in the case of ImageNet - InceptionResNetV2. As sCW binning creates ties at top predictions, the ACCs initially reported in Tab. 1 of Sec. 4.1 use the class index as the secondary sorting criterion. Here, we add  $\text{Acc}^*_{\text{top1}}$  and  $\text{Acc}^*_{\text{top5}}$  which are attained by using the raw logits as the secondary sorting criterion. As the CW ECEs are not affected by this change, here we only report the new  $\text{top1ECE}^*$ .

Binn.	$\text{Acc}_{\text{top1}} \uparrow$	$\text{Acc}^*_{\text{top1}} \uparrow$	$\text{Acc}_{\text{top5}} \uparrow$	$\text{Acc}^*_{\text{top5}} \uparrow$	$\text{top1ECE} \downarrow$	$\text{top1ECE}^* \downarrow$	NLL $\downarrow$
Baseline	<b>80.33</b>	-	<b>95.10</b>	-	0.0357	-	0.8406
Eq. Mass	5.02	<b>80.33</b>	26.75	<b>95.10</b>	0.0353	0.7884	3.5272
Eq. Size	80.14	80.21	88.99	<b>95.10</b>	0.0279	0.0277	1.2671
I-Max	80.20	<b>80.33</b>	94.86	<b>95.10</b>	<b>0.0200</b>	<b>0.0202</b>	<b>0.7860</b>

The second part of our post-hoc analysis is on the sCW binning strategy. When using the same binning scheme for all per-class calibration, the chance of creating ties in top- $k$  predictions is much higher than CW binning, e.g., more than one class are top-1 ranked according to the calibrated prediction probabilities. Our reported ACCs in the main paper are attained by simply returning the first found class, i.e., using the class index as the secondary sorting criterion. This is certainly a suboptimal solution. Here, we investigate on how the ties affect ACCs of sCW binning. To this end, we use raw logits (before binning) as the secondary sorting criterion. The resulting  $\text{ACC}^*_{\text{top1}}$  and  $\text{ACC}^*_{\text{top5}}$  are shown in Tab.S1. Interestingly, such a simple change reduces the accuracy loss of Eq. Mass and I-Max binning to zero, indicating that they can preserve the top-5 ranking order of the raw logits but not in a strict monotonic sense, i.e., some  $>$  are replaced by  $=$ . As opposed to I-Max binning, Eq. Mass binning has a poor performance at calibration, i.e., the really high NLL and ECE. This is because it trivially ranks many classes as top-1, but each of them has a very and same small confidence score. Given that, even though the accuracy loss is no longer an issue, it is still not a good solution for multi-class calibration. For Eq. Size binning, resolving ties only helps restore the baseline top-5 but not top-1 ACC. Its poor bin representative setting due to unreliable empirical frequency estimation over too narrow bins can result in a permutation among the top-5 predictions.

Concluding from the above, our post-hoc analysis confirms that I-Max binning outperforms the other two binning schemes at mitigating the accuracy loss and multi-class calibration. In particular, there exists a simple solution to close the accuracy gap to the baseline, at the same time still retaining the desirable calibration gains.

## S5 Ablation on the Number of Bins and Calibration Set Size

In Tab. 1 of Sec. 4.1, sCW I-Max binning is the top performing one at the ACCs, ECEs and NLL measures. In this part, we further investigate on how the number of bins and calibration set size influences its performance. Tab. S2 shows that in order to benefit from more bins we shall accordingly increase the number of calibration samples. More bins help reduce the quantization loss, but increase the empirical frequency estimation error for setting the bin representatives. Given that, we observe a reduced ACCs and increased ECEs for having 50 bins with only 1k calibration samples. By increasing the calibration set size to 5k, then we start seeing the benefits of having more bins to reduce quantization error for better ACCs. Next, we further exploit scaling method, i.e., GP [26], for improving the sample efficiency of binning at setting the bin representatives. As a result, the combination is particularly beneficial to improve the ACCs and top-1 ECE. Overall, more bins are beneficial to ACCs, while ECEs favor less number of bins.

## S6 Empirical ECE Estimation of Scaling Methods under Multiple Evaluation Schemes

As mentioned in the main paper, scaling methods suffer from not being able to provide verifiable ECEs, see Fig. 1. In Tab. S3 we adopt four different quantization schemes to empirically evaluate the ECEs of scaling methods. As we can see, the obtained results are evaluation scheme dependent. On contrary, I-Max binning with and without GP are not affected, and more importantly, their ECEs are better than that of scaling methods, regardless of the evaluation scheme.

Table S2: Ablation on the number of bins and calibration samples for sCW I-Max binning, where the basic setting is identical to the Tab. 1 in Sec. 4.1 of the main paper.

Binn.	Bins	Acc <sub>top1</sub> ↑	Acc <sub>top5</sub> ↑	cwECE <sub><math>\frac{1}{K}</math></sub> ↓	top1ECE ↓	Acc <sub>top1</sub> ↑	Acc <sub>top5</sub> ↑	cwECE <sub><math>\frac{1}{K}</math></sub> ↓	top1ECE ↓
Baseline	-	<b>80.33</b>	95.10	0.0486	0.0357	<b>80.33</b>	95.10	0.0486	0.0357
		1k Calibration Samples				5k Calibration Samples			
GP		<b>80.33</b>	<b>95.11</b>	0.0485	0.0186	<b>80.33</b>	<b>95.11</b>	0.0445	0.0177
I-Max	10	80.09	94.59	0.0316	0.0156	80.14	94.59	0.0330	0.0107
	15	80.20	94.86	0.0302	0.0200	80.21	94.90	0.0257	0.0107
	20	80.10	94.94	<b>0.0266</b>	0.0234	80.25	94.98	<b>0.0220</b>	0.0133
	30	80.15	94.99	0.0343	0.0266	80.25	95.02	0.0310	0.0150
	40	80.11	95.05	0.0365	0.0289	80.24	95.08	0.0374	0.0171
	50	80.21	94.95	0.0411	0.0320	80.23	95.06	0.0378	0.0219
I-Max w. GP	10	80.09	94.59	0.0396	0.0122	80.14	94.59	0.0330	<b>0.0072</b>
	15	80.20	94.87	0.0300	<b>0.0121</b>	80.21	94.88	0.0256	0.0080
	20	80.23	94.95	0.0370	0.0133	80.25	95.00	0.0270	0.0091
	30	80.26	95.04	0.0383	0.0141	80.27	95.02	0.0389	0.0097
	40	80.27	<b>95.11</b>	0.0424	0.0145	80.26	95.08	0.0402	0.0108
	50	80.30	95.08	0.0427	0.0153	80.28	95.08	0.0405	0.0114

Table S3: ECEs of scaling methods under various evaluation quantization schemes for ImageNet InceptionResNetV2. Overall, we consider four evaluation schemes, namely (1) dECE: equal size binning; (2) mECE: equal mass binning, (3) kECE: MSE-based KMeans clustering and (4) iECE: I-Max binning. All of them use  $10^2$  bins. Note that, the ECEs of I-Max binning (as a calibrator rather than evaluation scheme) are agnostic to the evaluation scheme, i.e., offering verifiable ECEs. Furthermore, BBQ suffers from severe accuracy degradation.

Calibrator	ACC <sub>top1</sub>	cw dECE <sub><math>\frac{1}{K}</math></sub> ↓	cw mECE <sub><math>\frac{1}{K}</math></sub> ↓	cw kECE <sub><math>\frac{1}{K}</math></sub> ↓	cw iECE <sub><math>\frac{1}{K}</math></sub> ↓	Mean ↓
Baseline	80.33	0.0486 ± 0.0003	0.0459 ± 0.0004	0.0484 ± 0.0004	0.0521 ± 0.0004	0.0488
25k Calibration Samples						
BBQ [19]	53.89	0.0287 ± 0.0009	0.0376 ± 0.0014	0.0372 ± 0.0014	0.0316 ± 0.0008	0.0338
Beta [11]	80.47	0.0706 ± 0.0003	0.0723 ± 0.0005	0.0742 ± 0.0005	0.0755 ± 0.0004	0.0732
Isotonic Reg. [30]	80.08	0.0644 ± 0.0015	0.0646 ± 0.0015	0.0652 ± 0.0016	0.0655 ± 0.0015	0.0649
Platt [21]	80.48	0.0597 ± 0.0007	0.0593 ± 0.0008	0.0613 ± 0.0008	0.0634 ± 0.0008	0.0609
Vec Scal. [12]	80.53	0.0494 ± 0.00020	0.0472 ± 0.0004	0.0498 ± 0.0003	0.0531 ± 0.0003	0.0499
Mtx Scal. [12]	<b>80.78</b>	0.0508 ± 0.0003	0.0488 ± 0.0004	0.0512 ± 0.0005	0.0544 ± 0.0004	0.0513
1k Calibration Samples						
TS [5]	80.33	0.0559 ± 0.0015	0.0548 ± 0.0018	0.0573 ± 0.0017	0.0598 ± 0.0015	0.0570
GP [26]	80.33	0.0485 ± 0.0037	0.0450 ± 0.0040	0.0475 ± 0.0039	0.0520 ± 0.0038	0.0483
I-Max	80.20	0.0302 ± 0.0041				
I-Max w. GP	80.20	<b>0.0300</b> ± 0.0041				
Calibrator	ACC <sub>top1</sub>	top1 dECE ↓	top1 mECE ↓	top1 kECE ↓	top1 iECE ↓	Mean ↓
Baseline	80.33	0.0357 ± 0.0010	0.0345 ± 0.0010	0.0348 ± 0.0012	0.0352 ± 0.0016	0.0351
25k Calibration Samples						
BBQ [19]	53.89	0.2689 ± 0.0033	0.2690 ± 0.0034	0.2690 ± 0.0034	0.2689 ± 0.0032	0.2689
Beta [11]	80.47	0.0346 ± 0.0022	0.0360 ± 0.0017	0.0360 ± 0.0022	0.0357 ± 0.0019	0.0356
Isotonic Reg. [30]	80.08	0.0468 ± 0.0020	0.0434 ± 0.0019	0.0436 ± 0.0020	0.0468 ± 0.0015	0.0452
Platt [21]	80.48	0.0775 ± 0.0015	0.0772 ± 0.0015	0.0771 ± 0.0016	0.0773 ± 0.0014	0.0772
Vec Scal. [12]	80.53	0.0300 ± 0.0010	0.0298 ± 0.0012	0.0300 ± 0.0016	0.0303 ± 0.0011	0.0300
Mtx Scal. [12]	<b>80.78</b>	0.0282 ± 0.0014	0.0287 ± 0.0011	0.0286 ± 0.0014	0.0289 ± 0.0014	0.0286
1k Calibration Samples						
TS [5]	80.33	0.0439 ± 0.0022	0.0452 ± 0.0022	0.0454 ± 0.0020	0.0443 ± 0.0020	0.0447
GP [26]	80.33	0.0186 ± 0.0034	0.0182 ± 0.0019	0.0186 ± 0.0026	0.0190 ± 0.0022	0.0186
I-Max	80.20	0.0200 ± 0.0033				
I-Max w. GP	80.20	<b>0.0121</b> ± 0.0048				

## S7 Training Details

### S7.1 Pre-trained Classification Networks

We evaluate post-hoc calibration methods on three benchmark datasets, i.e., ImageNet [3], CIFAR-100 [10], and CIFAR-10 [10], and across three modern DNNs for each dataset, i.e., InceptionResNetV2 [24], DenseNet161 [8] and ResNet152 [6] for ImageNet, and Wide ResNet (WRN) [31], DenseNet-BC ( $L = 190, k = 40$ ) [8] and ResNext8x64 [27] for the two CIFAR datasets.

All these models are publicly available pre-trained networks and details are reported at the respective websites, i.e., ImageNet classifiers: <https://github.com/Cadene/pretrained-models.pytorch> and CIFAR classifiers: <https://github.com/bearpaw/pytorch-classification>

### S7.2 Training Scaling Methods

The hyper-parameters were decided based on the original respective scaling methods publications with some exceptions. We found that the following parameters were the best for all the scaling methods. All scaling methods use the Adam optimizer with batch size 256 for CIFAR and 4096 for ImageNet. The learning rate was set to  $10^{-3}$  for temperature scaling [5] and Platt scaling [21], 0.0001 for vector scaling [5] and  $10^{-5}$  for matrix scaling [5]. Matrix scaling was further regularized as suggested by [12] with a  $L_2$  loss on the bias vector and the off-diagonal elements of the weighting matrix. BBQ [19], isotonic regression [30] and Beta [11] hyper-parameters were taken directly from [26].

### S7.3 Training I-Max Binning

The I-Max bin optimization started from k-means++ initialization, which uses JSD instead of Euclidean metric as the distance measure, see Sec. S3.2. Then, we iteratively and alternatively updated  $\{g_m\}$  and  $\{\phi_m\}$  according to (S12) until 200 iterations. With the attained bin edges  $\{g_m\}$ , we set the bin representatives  $\{r_m\}$  based on the empirical frequency of class-1. If a scaling method is combined with binning, an alternative setting for  $\{r_m\}$  is to take the averaged prediction probabilities based on the scaled logits of the samples per bin, e.g., in Tab. 2 of Sec. 4.2. Note that, for CW binning in Tab. 1, the number of samples from the minority class is too few, i.e.,  $25k/1k = 25$ . We only have about  $25/15 \approx 2$  samples per bin, which are too few to use empirical frequency estimates. Alternatively, we set  $\{r_m\}$  based on the raw prediction probabilities.

## S8 Extend Tab. 1 for More Datasets and Models.

Tab. 1 from Sec. 4.1 of the main paper is replicated across datasets and models, where the basic setting remains the same. Specifically, three different ImageNet models can be found in Tab. S4, Tab. S5 and Tab. S6. Three models for CIFAR100 can be found in Tab. S7, Tab. S8 and Tab. S9. Similarly, CIFAR10 models can be found in Tab. S10, Tab. S11 and Tab. S12. The accuracy degradation of Eq. Mass reduces as the dataset has less number of classes, e.g., CIFAR10. This is because the class imbalance under one-vs-rest conversion becomes less critical in CIFAR10 than ImageNet. Nevertheless, its accuracy losses are still much larger than the other binning schemes, i.e., Eq. Size and I-Max binning. Therefore, its calibration performance is not considered for comparison. Overall, the observations of Tab. S4- S12 are similar to Tab. 1, showing the stable performance gains of I-Max binning across datasets and models.

## S9 Extend Tab. 2 for More Scaling Methods, Datasets and Models

Tab. 2 from Sec. 4.2 of the main paper is replicated across datasets and models, and include more scaling methods for comparison. The three binning methods all use the shared CW strategy, therefore 1k calibration samples are sufficient. The basic setting remains the same as Tab. 2. Three different ImageNet models can be found in Tab. S13, Tab. S14 and Tab. S15. Three models for CIFAR100 can be found in Tab. S16, Tab. S17 and Tab. S18. Similarly, CIFAR10 models can be found in Tab. S19, Tab. S20 and Tab. S21.

Table S4: Tab. 1 Extension: ImageNet - InceptionResNetV2

Binn.	sCW(?)	size	Acc <sub>top1</sub> ↑	Acc <sub>top5</sub> ↑	cwECE <sub><math>\frac{1}{K}</math></sub> ↓	top1ECE ↓	NLL
Baseline	✗	-	<b>80.33</b> ± 0.15	<b>95.10</b> ± 0.15	0.0486 ± 0.0003	0.0357 ± 0.0009	0.8406 ± 0.0095
Eq. Mass	✗	25k	7.78 ± 0.15	27.92 ± 0.71	0.0016 ± 0.0001	0.0606 ± 0.0013	3.5960 ± 0.0137
Eq. Mass	✓	1k	5.02 ± 0.13	26.75 ± 0.37	0.0022 ± 0.0001	0.0353 ± 0.0012	3.5272 ± 0.0142
Eq. Size	✗	25k	78.52 ± 0.15	89.06 ± 0.13	0.1344 ± 0.0005	0.0547 ± 0.0017	1.5159 ± 0.0136
Eq. Size	✓	1k	80.14 ± 0.23	88.99 ± 0.12	0.1525 ± 0.0023	0.0279 ± 0.0043	1.2671 ± 0.0130
I-Max	✗	25k	80.27 ± 0.17	95.01 ± 0.19	0.0342 ± 0.0006	0.0329 ± 0.0010	0.8499 ± 0.0105
I-Max	✓	1k	80.20 ± 0.18	94.86 ± 0.17	<b>0.0302</b> ± 0.0041	<b>0.0200</b> ± 0.0033	<b>0.7860</b> ± 0.0208

Table S5: Tab. 1 Extension: ImageNet - DenseNet

Binn.	sCW(?)	size	Acc <sub>top1</sub> ↑	Acc <sub>top5</sub> ↑	cwECE <sub><math>\frac{1}{K}</math></sub> ↓	top1ECE ↓	NLL
Baseline	✗	-	<b>77.21</b> ± 0.12	<b>93.51</b> ± 0.14	0.0502 ± 0.0006	0.0571 ± 0.0014	0.9418 ± 0.0120
Eq. Mass	✗	25k	18.48 ± 0.19	45.12 ± 0.26	0.0017 ± 0.0000	0.1657 ± 0.0020	2.9437 ± 0.0162
Eq. Mass	✓	1k	17.21 ± 0.47	45.69 ± 1.22	0.0054 ± 0.0004	0.1572 ± 0.0047	2.9683 ± 0.0561
Eq. Size	✗	25k	74.34 ± 0.28	88.27 ± 0.11	0.1272 ± 0.0011	0.0660 ± 0.0018	1.6699 ± 0.0165
Eq. Size	✓	1k	77.06 ± 0.28	88.22 ± 0.10	0.1519 ± 0.0016	0.0230 ± 0.0050	1.3948 ± 0.0105
I-Max	✗	25k	77.07 ± 0.13	93.40 ± 0.17	0.0334 ± 0.0004	0.0577 ± 0.0008	0.9492 ± 0.0130
I-Max	✓	1k	77.13 ± 0.14	93.34 ± 0.17	<b>0.0263</b> ± 0.0119	<b>0.0201</b> ± 0.0088	<b>0.9229</b> ± 0.0103

Table S6: Tab. 1 Extension: ImageNet - ResNet152

Binn.	sCW(?)	size	Acc <sub>top1</sub> ↑	Acc <sub>top5</sub> ↑	cwECE <sub><math>\frac{1}{K}</math></sub> ↓	top1ECE ↓	NLL
Baseline	✗	-	<b>78.33</b> ± 0.17	<b>94.00</b> ± 0.14	0.0500 ± 0.0004	0.0512 ± 0.0018	0.8760 ± 0.0133
Eq. Mass	✗	25k	17.45 ± 0.10	44.87 ± 0.37	0.0017 ± 0.0000	0.1555 ± 0.0010	2.9526 ± 0.0168
Eq. Mass	✓	1k	16.25 ± 0.54	45.53 ± 0.81	0.0064 ± 0.0004	0.1476 ± 0.0054	2.9471 ± 0.0556
Eq. Size	✗	25k	75.50 ± 0.28	88.85 ± 0.19	0.1223 ± 0.0008	0.0604 ± 0.0017	1.6012 ± 0.0252
Eq. Size	✓	1k	78.24 ± 0.16	88.81 ± 0.19	0.1480 ± 0.0015	0.0286 ± 0.0053	1.3308 ± 0.0178
I-Max	✗	25k	78.24 ± 0.16	93.91 ± 0.17	0.0334 ± 0.0005	0.0521 ± 0.0015	0.8842 ± 0.0135
I-Max	✓	1k	78.19 ± 0.21	93.82 ± 0.17	<b>0.0295</b> ± 0.0030	<b>0.0196</b> ± 0.0049	<b>0.8638</b> ± 0.0135

Table S7: Tab. 1 Extension: CIFAR100 - WRN

Binn.	sCW(?)	size	Acc <sub>top1</sub> ↑	cwECE <sub><math>\frac{1}{K}</math></sub> ↓	top1ECE ↓	NLL
Baseline	✗	-	<b>81.35</b> ± 0.13	0.1113 ± 0.0010	0.0748 ± 0.0018	0.7816 ± 0.0076
Eq. Mass	✗	5k	60.78 ± 0.62	0.0129 ± 0.0010	0.4538 ± 0.0074	1.1084 ± 0.0117
Eq. Mass	✓	1k	62.04 ± 0.53	0.0252 ± 0.0032	0.4744 ± 0.0049	1.1789 ± 0.0308
Eq. Size	✗	5k	80.39 ± 0.36	0.1143 ± 0.0013	0.0783 ± 0.0032	1.0772 ± 0.0184
Eq. Size	✓	1k	81.12 ± 0.15	0.1229 ± 0.0030	0.0273 ± 0.0055	1.0165 ± 0.0105
I-Max	✗	5k	81.22 ± 0.12	0.0692 ± 0.0020	0.0751 ± 0.0024	0.7878 ± 0.0090
I-Max	✓	1k	81.30 ± 0.22	<b>0.0518</b> ± 0.0036	<b>0.0231</b> ± 0.0067	<b>0.7593</b> ± 0.0085

Table S8: Tab. 1 Extension: CIFAR100 - ResNeXt8x64

Binn.	sCW(?)	size	Acc <sub>top1</sub> ↑	cwECE <sub><math>\frac{1}{K}</math></sub> ↓	top1ECE ↓	NLL
Baseline	✗	-	81.93 ± 0.08	0.0979 ± 0.0015	0.0590 ± 0.0028	0.7271 ± 0.0026
Eq. Mass	✗	5k	63.02 ± 0.54	0.0131 ± 0.0012	0.4764 ± 0.0057	1.0535 ± 0.0191
Eq. Mass	✓	1k	64.48 ± 0.64	0.0265 ± 0.0011	0.4980 ± 0.0070	1.1232 ± 0.0277
Eq. Size	✗	5k	80.81 ± 0.26	0.1070 ± 0.0008	0.0700 ± 0.0030	1.0178 ± 0.0066
Eq. Size	✓	1k	81.99 ± 0.21	0.1195 ± 0.0013	0.0230 ± 0.0033	0.9556 ± 0.0071
I-Max	✗	5k	<b>81.99</b> ± 0.08	0.0601 ± 0.0027	0.0627 ± 0.0034	0.7318 ± 0.0026
I-Max	✓	1k	81.96 ± 0.14	<b>0.0549</b> ± 0.0081	<b>0.0205</b> ± 0.0074	<b>0.7127</b> ± 0.0040

Table S9: Tab. 1 Extension: CIFAR100 - DenseNet

Binn.	sCW(?)	size	Acc <sub>top1</sub> ↑	cwECE <sub><math>\frac{1}{K}</math></sub> ↓	top1ECE ↓	NLL
Baseline	✗	-	<b>82.36</b> ± 0.26	0.1223 ± 0.0008	0.0762 ± 0.0015	0.7542 ± 0.0143
Eq. Mass	✗	5k	57.23 ± 0.50	0.0117 ± 0.0011	0.4173 ± 0.0051	1.1819 ± 0.0228
Eq. Mass	✓	1k	58.11 ± 0.21	0.0233 ± 0.0005	0.4339 ± 0.0024	1.2049 ± 0.0405
Eq. Size	✗	5k	81.35 ± 0.23	0.1108 ± 0.0017	0.0763 ± 0.0029	1.0207 ± 0.0183
Eq. Size	✓	1k	82.22 ± 0.30	0.1192 ± 0.0024	0.0219 ± 0.0021	0.9482 ± 0.0137
I-Max	✗	5k	82.35 ± 0.26	0.0740 ± 0.0007	0.0772 ± 0.0010	0.7618 ± 0.0145
I-Max	✓	1k	82.32 ± 0.22	<b>0.0546</b> ± 0.0122	<b>0.0189</b> ± 0.0071	<b>0.7022</b> ± 0.0124

Table S10: Tab. 1 Extension: CIFAR10 - WRN

Binn.	sCW(?)	size	Acc <sub>top1</sub> ↑	cwECE <sub><math>\frac{1}{K}</math></sub> ↓	top1ECE ↓	NLL
Baseline	✗	-	<b>96.12</b> ± 0.14	0.0457 ± 0.0011	0.0288 ± 0.0007	0.1682 ± 0.0062
Eq. Mass	✗	5k	91.06 ± 0.54	0.0180 ± 0.0045	0.0794 ± 0.0066	0.2066 ± 0.0091
Eq. Mass	✓	1k	91.24 ± 0.27	0.0212 ± 0.0009	0.0836 ± 0.0091	0.2252 ± 0.0220
Eq. Size	✗	5k	96.04 ± 0.14	0.0344 ± 0.0008	0.0290 ± 0.0013	0.2231 ± 0.0074
Eq. Size	✓	1k	96.04 ± 0.15	0.0278 ± 0.0021	0.0105 ± 0.0028	0.2744 ± 0.0812
I-Max	✗	5k	96.10 ± 0.14	0.0329 ± 0.0011	0.0276 ± 0.0007	0.1704 ± 0.0067
I-Max	✓	1k	96.06 ± 0.13	<b>0.0304</b> ± 0.0012	<b>0.0113</b> ± 0.0039	<b>0.1595</b> ± 0.0604

Table S11: Tab. 1 Extension: CIFAR10 - ResNext8x64

Binn.	sCW(?)	size	Acc <sub>top1</sub> ↑	cwECE <sub><math>\frac{1}{K}</math></sub> ↓	top1ECE ↓	NLL
Baseline	✗	-	<b>96.30</b> ± 0.18	0.0485 ± 0.0014	0.0201 ± 0.0021	<b>0.1247</b> ± 0.0058
Eq. Mass	✗	5k	89.40 ± 0.55	0.0168 ± 0.0037	0.0589 ± 0.0052	0.2011 ± 0.0085
Eq. Mass	✓	1k	89.85 ± 0.61	0.0269 ± 0.0051	0.0676 ± 0.0127	0.2208 ± 0.0172
Eq. Size	✗	5k	96.30 ± 0.20	0.0274 ± 0.0013	0.0174 ± 0.0013	0.1613 ± 0.0101
Eq. Size	✓	1k	96.17 ± 0.24	0.0288 ± 0.0039	0.0114 ± 0.0025	0.2495 ± 0.0571
I-Max	✗	5k	96.26 ± 0.20	<b>0.0240</b> ± 0.0020	0.0167 ± 0.0014	0.1264 ± 0.0066
I-Max	✓	1k	96.22 ± 0.21	0.0254 ± 0.0030	<b>0.0104</b> ± 0.0025	0.1397 ± 0.0276

Table S12: Tab. 1 Extension Dataset: CIFAR10 - DenseNet

Binn.	sCW(?)	size	Acc <sub>top1</sub> ↑	cwECE <sub><math>\frac{1}{K}</math></sub> ↓	top1ECE ↓	NLL
Baseline	✗	-	96.65 ± 0.09	0.0404 ± 0.001	0.0253 ± 0.0009	0.1564 ± 0.0075
Eq. Mass	✓	1k	88.80 ± 0.47	0.0233 ± 0.0024	0.0637 ± 0.0023	0.2694 ± 0.0274
Eq. Mass	✗	5k	89.51 ± 0.36	0.0137 ± 0.0039	0.0657 ± 0.0041	0.2283 ± 0.0101
Eq. Size	✓	1k	96.64 ± 0.22	0.0262 ± 0.0035	0.0101 ± 0.0035	0.2465 ± 0.0543
Eq. Size	✗	5k	96.74 ± 0.07	0.0301 ± 0.0012	0.0242 ± 0.0013	0.1912 ± 0.0075
I-Max	✓	1k	96.59 ± 0.32	0.0261 ± 0.0025	0.0098 ± 0.0027	0.1208 ± 0.0044
I-Max	✗	5k	96.71 ± 0.09	0.0284 ± 0.0013	0.0233 ± 0.0009	0.1608 ± 0.0086

Table S13: Tab. 2 Extension: ImageNet - InceptionResnetV2

Calibrator	Acc <sub>top1</sub> ↑	Acc <sub>top5</sub> ↑	cwECE $\frac{1}{K}$ ↓	top1ECE ↓	NLL	Brier
Baseline	80.33 ± 0.15	95.10 ± 0.15	0.0486 ± 0.0003	0.0357 ± 0.0009	0.8406 ± 0.0095	0.1115 ± 0.0007
25k Calibration Samples						
BBQ [19]	53.89 ± 0.30	88.63 ± 0.22	0.0287 ± 0.0009	0.2689 ± 0.0033	1.7104 ± 0.0370	0.3273 ± 0.0016
Beta [11]	80.47 ± 0.14	94.84 ± 0.15	0.0706 ± 0.0003	0.0346 ± 0.0022	0.9038 ± 0.0270	0.1174 ± 0.0010
Isotonic Reg. [30]	80.08 ± 0.19	93.46 ± 0.20	0.0644 ± 0.0014	0.0468 ± 0.0020	1.8375 ± 0.0587	0.1203 ± 0.0012
Platt [21]	80.48 ± 0.14	95.18 ± 0.12	0.0597 ± 0.0007	0.0775 ± 0.0015	0.8083 ± 0.0106	0.1205 ± 0.0010
VUC [13]	6.72 ± 0.21	27.36 ± 0.15	0.0012 ± 0.0001	0.0489 ± 0.0022	3.9514 ± 0.0186	0.0653 ± 0.0021
Vec Scal. [12]	80.53 ± 0.19	95.18 ± 0.16	0.0494 ± 0.0002	0.0300 ± 0.0010	0.8269 ± 0.0097	0.1106 ± 0.0007
Mtx Scal. [12]	<b>80.78</b> ± 0.18	<b>95.38</b> ± 0.15	0.0508 ± 0.0003	0.0282 ± 0.0014	0.8042 ± 0.0100	0.1090 ± 0.0006
1k Calibration Samples						
TS [5]	80.33 ± 0.16	95.10 ± 0.16	0.0559 ± 0.0015	0.0439 ± 0.0022	0.8293 ± 0.0107	0.1134 ± 0.0010
GP [26]	80.33 ± 0.15	95.11 ± 0.15	0.0485 ± 0.0035	0.0186 ± 0.0034	<b>0.7556</b> ± 0.0118	<b>0.1069</b> ± 0.0017
Eq. Mass	5.02 ± 0.13	26.75 ± 0.37	0.0022 ± 0.0001	0.0353 ± 0.0012	3.5272 ± 0.0142	0.0489 ± 0.0012
Eq. Size	80.14 ± 0.23	88.99 ± 0.12	0.1525 ± 0.0023	0.0279 ± 0.0043	1.2671 ± 0.0130	0.1115 ± 0.0011
I-Max	80.20 ± 0.18	94.86 ± 0.17	0.0302 ± 0.0041	0.0200 ± 0.0033	0.7860 ± 0.0208	0.1116 ± 0.0008
Eq. Mass w. TS	5.02 ± 0.13	26.87 ± 0.43	0.0023 ± 0.0001	0.0357 ± 0.0012	3.5454 ± 0.0222	0.0490 ± 0.0012
Eq. Mass w. GP	5.02 ± 0.13	26.87 ± 0.43	0.0022 ± 0.0001	0.0353 ± 0.0012	3.4778 ± 0.0217	0.0489 ± 0.0012
Eq. Size w. TS	80.26 ± 0.18	88.99 ± 0.12	0.1470 ± 0.0007	0.0391 ± 0.0038	1.2721 ± 0.0116	0.1136 ± 0.0012
Eq. Size w. GP	80.26 ± 0.18	88.99 ± 0.12	0.1508 ± 0.0021	0.0140 ± 0.0056	1.2661 ± 0.0121	0.1105 ± 0.0008
I-Max w. TS	80.20 ± 0.18	94.87 ± 0.19	0.0354 ± 0.0124	0.0402 ± 0.0019	0.8339 ± 0.0108	0.1142 ± 0.0009
I-Max w. GP	80.20 ± 0.18	94.87 ± 0.19	<b>0.0300</b> ± 0.0041	<b>0.0121</b> ± 0.0048	0.7787 ± 0.0102	0.1111 ± 0.0006

Table S14: Tab. 2 Extension: ImageNet - DenseNet

Calibrator	Acc <sub>top1</sub> ↑	Acc <sub>top5</sub> ↑	cwECE $\frac{1}{K}$ ↓	top1ECE ↓	NLL	Brier
Baseline	77.21 ± 0.12	93.51 ± 0.14	0.0502 ± 0.0006	0.0571 ± 0.0014	0.9418 ± 0.0120	0.1228 ± 0.0009
25k Calibration Samples						
BBQ [19]	54.69 ± 0.42	86.55 ± 0.19	0.0274 ± 0.0007	0.2819 ± 0.0050	1.9805 ± 0.0500	0.3355 ± 0.0026
Beta [11]	77.35 ± 0.22	93.34 ± 0.17	0.0494 ± 0.0008	0.0253 ± 0.0022	0.9768 ± 0.0254	0.1209 ± 0.0010
Isotonic Reg. [30]	76.81 ± 0.24	91.98 ± 0.17	0.0577 ± 0.0003	0.0490 ± 0.0021	1.9819 ± 0.0634	0.1281 ± 0.0012
Platt [21]	77.43 ± 0.21	93.64 ± 0.15	0.0448 ± 0.0010	0.0906 ± 0.0022	0.9168 ± 0.0139	0.1297 ± 0.0012
VUC [13]	17.98 ± 0.24	45.65 ± 0.33	0.0014 ± 0.0001	0.1607 ± 0.0026	2.9832 ± 0.0228	0.1742 ± 0.0023
Vec Scal. [12]	77.44 ± 0.20	93.62 ± 0.17	0.0492 ± 0.0006	0.0516 ± 0.0018	0.9276 ± 0.0134	0.1208 ± 0.0011
Mtx Scal. [12]	<b>77.56</b> ± 0.11	<b>93.81</b> ± 0.15	0.0498 ± 0.0006	0.0491 ± 0.0015	0.9159 ± 0.0158	0.1202 ± 0.0016
1k Calibration Samples						
TS [5]	77.21 ± 0.12	93.51 ± 0.15	0.0375 ± 0.0007	0.0300 ± 0.0019	0.9116 ± 0.0110	0.1197 ± 0.0008
GP [26]	77.22 ± 0.12	93.51 ± 0.13	0.0394 ± 0.0037	0.0268 ± 0.0035	<b>0.8914</b> ± 0.0120	<b>0.1188</b> ± 0.0005
Eq. Mass	17.21 ± 0.47	45.69 ± 1.22	0.0054 ± 0.0004	0.1572 ± 0.0047	2.9683 ± 0.0561	0.1671 ± 0.0046
Eq. Size	77.06 ± 0.28	88.22 ± 0.10	0.1519 ± 0.0016	0.0230 ± 0.0050	1.3948 ± 0.0105	0.1206 ± 0.0013
I-Max	77.13 ± 0.14	93.34 ± 0.17	0.0263 ± 0.0119	0.0201 ± 0.0088	0.9229 ± 0.0103	0.1201 ± 0.0010
Eq. Mass w. TS	17.21 ± 0.47	45.73 ± 1.07	0.0054 ± 0.0004	0.1571 ± 0.0047	2.9104 ± 0.0482	0.1671 ± 0.0046
Eq. Mass w. GP	17.21 ± 0.47	45.71 ± 1.08	0.0054 ± 0.0004	0.1571 ± 0.0047	2.9090 ± 0.0485	0.1671 ± 0.0046
Eq. Size w. TS	77.19 ± 0.12	88.22 ± 0.10	0.1464 ± 0.0005	0.0241 ± 0.0032	1.3928 ± 0.0106	0.1201 ± 0.0008
Eq. Size w. GP	77.19 ± 0.12	88.22 ± 0.10	0.1527 ± 0.0007	0.0215 ± 0.0037	1.3944 ± 0.0094	0.1200 ± 0.0005
I-Max w. TS	77.13 ± 0.14	93.34 ± 0.17	0.0320 ± 0.0026	0.0245 ± 0.0024	0.9242 ± 0.0117	0.1201 ± 0.0007
I-Max w. GP	77.13 ± 0.14	93.34 ± 0.17	<b>0.0258</b> ± 0.0100	<b>0.0204</b> ± 0.0021	0.9200 ± 0.0124	0.1201 ± 0.0005

Being analogous to Tab. 2, we observe that in most cases matrix scaling performs the best at the accuracy, but fail to provide satisfactory calibration performance measured by ECEs, Brier scores and NLLs. Among the scaling methods, GP [26] is the top performing one. Among the binning schemes, our proposal of I-Max binning outperforms Eq. Mass and Eq. Size at both calibration and accuracy. The combination of I-Max binning with GP excels at the ECE performance. It achieves slightly worse results than GP alone at Brier scores and NLLs. This relates to the reduced precision of prediction probabilities after binning. Note that, among all methods, Eq. Mass binning and VUC [13] suffer from severe accuracy degradation after multi-class calibration. The reason behind Eq. Mass binning was discussed in Sec. 3.3 of the main paper. As VUC [13] combined Eq. Mass binning with Platt scaling, its accuracy loss is due to the same reason. Given their poor accuracy, they are not in the scope of calibration performance comparison.

Table S15: Tab. 2 Extension: ImageNet - ResNet152

Calibrator	Acc <sub>top1</sub> ↑	Acc <sub>top5</sub> ↑	cwECE $\frac{1}{K}$ ↓	top1 ECE ↓	NLL	Brier
Baseline	78.33 ± 0.17	94.00 ± 0.14	0.05 ± 0.0004	0.0512 ± 0.0018	0.8760 ± 0.0133	0.1174 ± 0.0013
25k Calibration Samples						
BBQ [19]	55.04 ± 0.26	87.15 ± 0.21	0.0278 ± 0.0004	0.2840 ± 0.0028	1.8490 ± 0.0474	0.3361 ± 0.0014
Beta [11]	78.44 ± 0.16	93.71 ± 0.20	0.0507 ± 0.0012	0.0264 ± 0.0010	0.9365 ± 0.0249	0.1174 ± 0.0013
Isotonic Reg. [30]	77.97 ± 0.07	92.33 ± 0.32	0.0590 ± 0.0016	0.0486 ± 0.0027	1.9437 ± 0.1020	0.1248 ± 0.0015
Platt [21]	78.56 ± 0.15	94.06 ± 0.19	0.0458 ± 0.0009	0.0852 ± 0.0021	0.8557 ± 0.0159	0.1246 ± 0.0015
VUC [13]	16.50 ± 0.13	45.11 ± 0.42	0.0013 ± 0.0000	0.1463 ± 0.0012	2.9838 ± 0.0154	0.1599 ± 0.0012
Vec Scal. [12]	<b>78.61</b> ± 0.21	94.12 ± 0.18	0.0490 ± 0.0003	0.0469 ± 0.0017	0.8625 ± 0.0143	0.1159 ± 0.0012
Mtx Scal. [12]	78.54 ± 0.23	<b>94.14</b> ± 0.22	0.0496 ± 0.0004	0.0443 ± 0.0026	0.8583 ± 0.0180	0.1160 ± 0.0016
1k Calibration Samples						
TS [5]	78.33 ± 0.18	94.00 ± 0.15	0.0378 ± 0.0007	0.0285 ± 0.0023	0.8505 ± 0.0126	0.1147 ± 0.0012
GP [26]	78.33 ± 0.17	94.00 ± 0.14	0.0403 ± 0.0021	0.0202 ± 0.0030	<b>0.8366</b> ± 0.0118	<b>0.1138</b> ± 0.0012
Eq. Mass	16.25 ± 0.54	45.53 ± 0.81	0.0064 ± 0.0004	0.1476 ± 0.0054	2.9471 ± 0.0556	0.1579 ± 0.0052
Eq. Size	78.24 ± 0.16	88.81 ± 0.19	0.1480 ± 0.0015	0.0286 ± 0.0053	1.3308 ± 0.0178	0.1167 ± 0.0011
I-Max	78.19 ± 0.21	93.82 ± 0.17	0.0295 ± 0.0030	0.0196 ± 0.0049	0.8638 ± 0.0135	0.1157 ± 0.0012
Eq. Mass w. TS	16.25 ± 0.54	45.54 ± 0.71	0.0064 ± 0.0004	0.1476 ± 0.0054	2.9024 ± 0.0401	0.1579 ± 0.0052
Eq. Mass w. GP	16.25 ± 0.54	45.52 ± 0.74	0.0064 ± 0.0004	0.1475 ± 0.0054	2.9021 ± 0.0400	0.1579 ± 0.0052
Eq. Size w. TS	78.27 ± 0.17	88.81 ± 0.19	0.1428 ± 0.0007	0.0225 ± 0.0022	1.3286 ± 0.0171	0.1153 ± 0.0013
Eq. Size w. GP	78.27 ± 0.17	88.81 ± 0.19	0.1475 ± 0.0016	0.0138 ± 0.0049	1.330 ± 0.0171	0.1150 ± 0.0012
I-Max w. TS	78.19 ± 0.21	93.82 ± 0.17	<b>0.0281</b> ± 0.0029	0.0219 ± 0.0016	0.8637 ± 0.0125	0.1152 ± 0.0015
I-Max w. GP	78.19 ± 0.21	93.82 ± 0.17	0.0296 ± 0.0029	<b>0.0144</b> ± 0.0050	0.8602 ± 0.0127	0.1150 ± 0.0014

Table S16: Tab. 2 Extension: CIFAR100 - WRN

Calibrator	Acc <sub>top1</sub> ↑	cwECE $\frac{1}{K}$ ↓	top1 ECE ↓	NLL	Brier
Baseline	81.35 ± 0.13	0.1113 ± 0.0010	0.0748 ± 0.0018	0.7816 ± 0.0076	0.1082 ± 0.0021
5k Calibration Samples					
BBQ [19]	80.44 ± 0.19	0.0576 ± 0.0018	0.0672 ± 0.0044	1.7976 ± 0.0443	0.1297 ± 0.0019
Beta [11]	81.44 ± 0.17	0.0952 ± 0.0006	0.0379 ± 0.0027	0.7624 ± 0.0148	0.1018 ± 0.0016
Isotonic Reg. [30]	81.25 ± 0.27	0.0597 ± 0.0029	0.0487 ± 0.0040	1.4015 ± 0.0748	0.1059 ± 0.0013
Platt [21]	81.35 ± 0.12	0.0827 ± 0.0014	0.0585 ± 0.0038	0.7491 ± 0.0073	0.1026 ± 0.0017
VUC [13]	61.92 ± 1.11	0.0104 ± 0.0008	0.4660 ± 0.0110	1.1901 ± 0.0231	0.4570 ± 0.0079
Vec Scal. [12]	81.35 ± 0.21	0.1063 ± 0.0013	0.0687 ± 0.0029	0.7619 ± 0.0064	0.1055 ± 0.0017
Mtx Scal. [12]	<b>81.44</b> ± 0.20	0.1085 ± 0.0008	0.0692 ± 0.0033	0.7531 ± 0.0078	0.1059 ± 0.0019
1k Calibration Samples					
TS [5]	81.35 ± 0.14	0.0911 ± 0.0036	0.0511 ± 0.0059	0.7527 ± 0.0074	0.1036 ± 0.0025
Eq. Mass	62.04 ± 0.53	0.0252 ± 0.0032	0.4744 ± 0.0049	1.1789 ± 0.0308	0.4606 ± 0.0034
GP [26]	81.34 ± 0.12	0.1074 ± 0.0043	0.0358 ± 0.0039	<b>0.6943</b> ± 0.0025	<b>0.0996</b> ± 0.0019
Eq. Size	81.12 ± 0.15	0.1229 ± 0.0030	0.0273 ± 0.0055	1.0165 ± 0.0105	0.1039 ± 0.0017
I-Max	81.30 ± 0.22	0.0518 ± 0.0036	0.0231 ± 0.0067	0.7593 ± 0.0085	0.1016 ± 0.0018
Eq. Mass w. TS	62.04 ± 0.53	0.0253 ± 0.0034	0.4764 ± 0.0052	1.0990 ± 0.0184	0.4624 ± 0.0037
Eq. Mass w. GP	62.04 ± 0.53	0.0252 ± 0.0032	0.4749 ± 0.0051	1.1110 ± 0.0226	0.4610 ± 0.0036
Eq. Size w. TS	81.31 ± 0.15	0.1197 ± 0.0029	0.0362 ± 0.0065	1.0106 ± 0.0113	0.1038 ± 0.0026
Eq. Size w. GP	81.31 ± 0.15	0.1205 ± 0.0025	0.0189 ± 0.0054	1.0161 ± 0.0115	0.1032 ± 0.0020
I-Max w. TS	81.34 ± 0.20	<b>0.051</b> ± 0.0035	0.0365 ± 0.0067	0.7716 ± 0.0066	0.1025 ± 0.0021
I-Max w. GP	81.34 ± 0.20	0.0559 ± 0.0089	<b>0.0179</b> ± 0.0046	0.7609 ± 0.0080	0.1014 ± 0.0014

Table S17: Tab. 2 Extension: CIFAR100 - ResNeXt

Calibrator	Acc <sub>top1</sub> ↑	cwECE <sub><math>\frac{1}{K}</math></sub> ↓	top1ECE ↓	NLL	Brier
Baseline	81.93 ± 0.08	0.0979 ± 0.0015	0.0590 ± 0.0028	0.7271 ± 0.0026	0.0984 ± 0.0022
5k Calibration Samples					
BBQ [19]	81.06 ± 0.30	0.0564 ± 0.0013	0.0608 ± 0.0058	1.6878 ± 0.0546	0.1176 ± 0.0022
Beta [11]	82.19 ± 0.31	0.0918 ± 0.0020	0.0368 ± 0.0047	0.7095 ± 0.0074	0.0947 ± 0.0024
Isotonic Reg. [30]	81.89 ± 0.19	0.0619 ± 0.0023	0.0503 ± 0.0036	1.3015 ± 0.0656	0.0995 ± 0.0018
Platt [21]	82.28 ± 0.21	0.0790 ± 0.0025	0.0534 ± 0.0047	0.7050 ± 0.0045	0.0961 ± 0.0026
VUC [13]	64.24 ± 0.62	0.0109 ± 0.0017	0.4896 ± 0.0059	1.1010 ± 0.0237	0.4729 ± 0.0046
Vec Scal. [12]	82.24 ± 0.27	0.0963 ± 0.0013	0.0572 ± 0.0037	0.7129 ± 0.0053	0.0973 ± 0.0021
Mtx Scal. [12]	<b>82.38</b> ± 0.17	0.0970 ± 0.0014	0.0578 ± 0.0040	0.7042 ± 0.0046	0.0973 ± 0.0023
1k Calibration Samples					
TS [5]	81.93 ± 0.08	0.0864 ± 0.0036	0.0525 ± 0.0057	0.7163 ± 0.0037	0.0975 ± 0.0020
GP [26]	81.93 ± 0.09	0.1025 ± 0.0037	0.0345 ± 0.0038	<b>0.6456</b> ± 0.0071	<b>0.0927</b> ± 0.0019
Eq. Mass	64.48 ± 0.64	0.0265 ± 0.0011	0.4980 ± 0.0070	1.1232 ± 0.0277	0.4770 ± 0.0051
Eq. Size	81.99 ± 0.21	0.1195 ± 0.0013	0.0230 ± 0.0033	0.9556 ± 0.0071	0.0974 ± 0.0014
I-Max	81.96 ± 0.14	0.0549 ± 0.0081	0.0205 ± 0.0074	0.7127 ± 0.0040	0.0959 ± 0.0018
Eq. Mass w. TS	64.48 ± 0.64	0.0262 ± 0.0013	0.5003 ± 0.0066	1.0468 ± 0.0228	0.4793 ± 0.0048
Eq. Mass w. GP	64.48 ± 0.64	0.0264 ± 0.0012	0.4986 ± 0.0066	1.0555 ± 0.0227	0.4776 ± 0.0048
Eq. Size w. TS	81.94 ± 0.09	0.1179 ± 0.0015	0.0343 ± 0.0029	0.9498 ± 0.0058	0.0968 ± 0.0022
Eq. Size w. GP	81.94 ± 0.09	0.1177 ± 0.0009	0.0151 ± 0.0029	0.9561 ± 0.0056	0.0959 ± 0.0018
I-Max w. TS	81.96 ± 0.14	<b>0.053</b> ± 0.0073	0.0333 ± 0.0023	0.7286 ± 0.0029	0.0964 ± 0.0019
I-Max w. GP	81.96 ± 0.14	0.0532 ± 0.0077	<b>0.0121</b> ± 0.0026	0.7111 ± 0.0024	0.0950 ± 0.0017

Table S18: Tab. 2 Extension Dataset: CIFAR100 - DenseNet

Calibrator	Acc <sub>top1</sub> ↑	cwECE <sub><math>\frac{1}{K}</math></sub> ↓	top1ECE ↓	NLL	Brier
Baseline	82.36 ± 0.26	0.1223 ± 0.0008	0.0762 ± 0.0015	0.7542 ± 0.0143	0.1041 ± 0.0008
5k Calibration Samples					
BBQ [19]	81.56 ± 0.22	0.0567 ± 0.0020	0.0635 ± 0.0052	1.5876 ± 0.0914	0.1216 ± 0.0026
Beta [11]	82.39 ± 0.28	0.0953 ± 0.0013	0.0364 ± 0.0034	0.6935 ± 0.0185	0.0966 ± 0.0008
Isotonic Reg. [30]	82.05 ± 0.26	0.0591 ± 0.0016	0.0506 ± 0.0025	1.3030 ± 0.1107	0.1019 ± 0.0014
Platt [21]	82.34 ± 0.28	0.0866 ± 0.0012	0.0491 ± 0.0012	0.6835 ± 0.0138	0.0969 ± 0.0015
VUC [13]	58.32 ± 0.90	0.0099 ± 0.0008	0.4308 ± 0.0086	1.2175 ± 0.0117	0.4324 ± 0.0065
Vec Scal. [12]	82.38 ± 0.32	0.1195 ± 0.0005	0.0711 ± 0.0015	0.7362 ± 0.0173	0.1028 ± 0.0015
Mtx Scal. [12]	<b>82.53</b> ± 0.19	0.1214 ± 0.0006	0.0733 ± 0.0013	0.7360 ± 0.0153	0.1025 ± 0.0015
1k Calibration Samples					
TS [5]	82.36 ± 0.27	0.0938 ± 0.0017	0.0447 ± 0.0023	0.6851 ± 0.0115	0.0976 ± 0.0008
GP [26]	82.35 ± 0.27	0.1021 ± 0.0032	0.0338 ± 0.0011	<b>0.6536</b> ± 0.0120	<b>0.0943</b> ± 0.0007
Eq. Mass	58.11 ± 0.21	0.0233 ± 0.0005	0.4339 ± 0.0024	1.2049 ± 0.0405	0.4317 ± 0.0017
Eq. Size	82.22 ± 0.30	0.1192 ± 0.0024	0.0219 ± 0.0021	0.9482 ± 0.0137	0.0997 ± 0.0014
I-Max	82.32 ± 0.22	0.0546 ± 0.0122	0.0189 ± 0.0071	0.7022 ± 0.0124	0.0967 ± 0.0019
Eq. Mass w. TS	58.11 ± 0.21	0.0233 ± 0.0006	0.4347 ± 0.0024	1.1483 ± 0.0102	0.4324 ± 0.0017
Eq. Mass w. GP	58.11 ± 0.21	0.0233 ± 0.0005	0.4342 ± 0.0024	1.1508 ± 0.0099	0.4319 ± 0.0018
Eq. Size w. TS	82.40 ± 0.24	0.1134 ± 0.0014	0.0245 ± 0.0025	0.9427 ± 0.0137	0.0986 ± 0.0013
Eq. Size w. GP	82.40 ± 0.24	0.1166 ± 0.0021	0.0126 ± 0.0012	0.9455 ± 0.0142	0.0985 ± 0.0013
I-Max w. TS	82.36 ± 0.21	<b>0.048</b> ± 0.0090	0.0237 ± 0.0009	0.7040 ± 0.0104	0.0967 ± 0.0010
I-Max w. GP	82.36 ± 0.21	0.0535 ± 0.0121	<b>0.0114</b> ± 0.0025	0.6988 ± 0.0104	0.0964 ± 0.0010

Table S19: Tab. 2 Extension: CIFAR10 - WRN

Calibrator	Acc <sub>top1</sub> ↑	cwECE <sub><math>\frac{1}{K}</math></sub> ↓	top1ECE ↓	NLL	Brier
Baseline	96.12 ± 0.14	0.0457 ± 0.0011	0.0288 ± 0.0007	0.1682 ± 0.0062	0.0307 ± 0.0008
5k Calibration Samples					
BBQ [19]	95.98 ± 0.15	0.0290 ± 0.0047	0.0198 ± 0.0044	0.2054 ± 0.0156	0.0314 ± 0.0005
Beta [11]	96.31 ± 0.06	0.0504 ± 0.0015	0.0208 ± 0.0023	0.1335 ± 0.0039	0.0271 ± 0.0007
Isotonic Reg. [30]	96.20 ± 0.12	0.0241 ± 0.0021	0.0138 ± 0.0017	0.1764 ± 0.0241	0.0273 ± 0.0005
Platt [21]	96.24 ± 0.09	0.0489 ± 0.0011	0.0177 ± 0.0015	0.1359 ± 0.0039	0.0270 ± 0.0006
VUC [13]	90.18 ± 0.48	0.0213 ± 0.0036	0.0817 ± 0.0052	0.2256 ± 0.0075	0.0867 ± 0.0026
Vec Scal. [12]	<b>96.27</b> ± 0.11	0.0449 ± 0.0008	0.0229 ± 0.0008	0.1437 ± 0.0050	0.0286 ± 0.0007
Mtx Scal. [12]	96.20 ± 0.10	0.0444 ± 0.0005	0.0277 ± 0.0007	0.1625 ± 0.0062	0.0302 ± 0.0008
1k Calibration Samples					
TS [5]	96.12 ± 0.14	0.0486 ± 0.0024	0.0205 ± 0.0009	0.1385 ± 0.0048	0.0278 ± 0.0007
GP [26]	96.10 ± 0.13	0.0549 ± 0.0021	0.0146 ± 0.0022	<b>0.1281</b> ± 0.0055	0.0269 ± 0.0009
Eq. Mass	91.24 ± 0.27	0.0212 ± 0.0009	0.0836 ± 0.0091	0.2252 ± 0.0220	0.0858 ± 0.0055
Eq. Size	96.04 ± 0.15	0.0278 ± 0.0021	0.0105 ± 0.0028	0.2744 ± 0.0812	0.0305 ± 0.0015
I-Max	96.06 ± 0.13	0.0304 ± 0.0012	0.0113 ± 0.0039	0.1595 ± 0.0604	0.0274 ± 0.0013
Eq. Mass w. TS	91.24 ± 0.27	0.0219 ± 0.0005	0.0837 ± 0.0092	0.1944 ± 0.0093	0.0853 ± 0.0054
Eq. Mass w. GP	91.24 ± 0.27	0.0212 ± 0.0008	0.0821 ± 0.0088	0.1918 ± 0.0091	0.0851 ± 0.0054
Eq. Size w. TS	96.13 ± 0.12	0.0286 ± 0.0018	0.0125 ± 0.0024	0.1940 ± 0.0063	0.0296 ± 0.0009
Eq. Size w. GP	96.13 ± 0.11	<b>0.0266</b> ± 0.0016	<b>0.0066</b> ± 0.0028	0.1917 ± 0.0058	0.0292 ± 0.0009
I-Max w. TS	96.14 ± 0.13	0.0293 ± 0.0010	0.0163 ± 0.0012	0.1417 ± 0.0047	0.0280 ± 0.0008
I-Max w. GP	96.14 ± 0.13	0.0276 ± 0.0011	0.0074 ± 0.0035	0.1331 ± 0.0042	<b>0.0268</b> ± 0.0008

Table S20: Tab. 2 Extension: CIFAR10 - ResNeXt

Calibrator	Acc <sub>top1</sub> ↑	cwECE <sub><math>\frac{1}{K}</math></sub> ↓	top1ECE ↓	NLL	Brier
Baseline	96.30 ± 0.18	0.0485 ± 0.0014	0.0201 ± 0.0021	0.1247 ± 0.0058	0.0266 ± 0.0013
5k Calibration Samples					
BBQ [19]	96.18 ± 0.12	0.0256 ± 0.0027	0.0166 ± 0.0020	0.1951 ± 0.0134	0.0286 ± 0.0004
Beta [11]	96.31 ± 0.22	0.0517 ± 0.0011	0.0148 ± 0.0016	0.1163 ± 0.0040	0.0256 ± 0.0011
Isotonic Reg. [30]	96.35 ± 0.20	0.0241 ± 0.0016	0.0129 ± 0.0008	0.1686 ± 0.0099	0.0264 ± 0.0011
Platt [21]	96.34 ± 0.19	0.0511 ± 0.0008	0.0143 ± 0.0017	0.1159 ± 0.0042	0.0256 ± 0.0011
VUC [13]	89.17 ± 0.40	0.0141 ± 0.0028	0.0589 ± 0.0042	0.1999 ± 0.0076	0.0837 ± 0.0011
Vec Scal. [12]	<b>96.37</b> ± 0.19	0.0495 ± 0.0017	0.0161 ± 0.0017	0.1189 ± 0.0053	0.0258 ± 0.0013
Mtx Scal. [12]	96.34 ± 0.21	0.0492 ± 0.0020	0.0187 ± 0.0020	0.1225 ± 0.0060	0.0263 ± 0.0014
1k Calibration Samples					
TS [5]	96.30 ± 0.19	0.0524 ± 0.0028	0.0150 ± 0.0009	0.1182 ± 0.0051	0.0257 ± 0.0012
GP [26]	96.31 ± 0.17	0.0529 ± 0.0017	0.0125 ± 0.0021	<b>0.1176</b> ± 0.0051	<b>0.0258</b> ± 0.0011
Eq. Mass	89.85 ± 0.61	0.0269 ± 0.0051	0.0676 ± 0.0127	0.2208 ± 0.0172	0.0841 ± 0.0042
Eq. Size	96.17 ± 0.24	0.0288 ± 0.0039	0.0114 ± 0.0025	0.2495 ± 0.0571	0.0277 ± 0.0008
I-Max	96.22 ± 0.21	0.0254 ± 0.0030	0.0104 ± 0.0025	0.1397 ± 0.0276	0.0265 ± 0.0012
Eq. Mass w. TS	89.85 ± 0.61	0.0269 ± 0.0054	0.0676 ± 0.0128	0.1966 ± 0.0104	0.0844 ± 0.0043
Eq. Mass w. GP	89.85 ± 0.61	0.0266 ± 0.0049	0.0669 ± 0.0126	0.1962 ± 0.0106	0.0841 ± 0.0043
Eq. Size w. TS	96.29 ± 0.18	0.0270 ± 0.0022	0.0062 ± 0.0024	0.1574 ± 0.0091	0.0264 ± 0.0013
Eq. Size w. GP	96.29 ± 0.18	0.0271 ± 0.0020	0.0063 ± 0.0030	0.1576 ± 0.0093	0.0264 ± 0.0012
I-Max w. TS	96.28 ± 0.19	0.0224 ± 0.0016	0.0053 ± 0.0024	0.1208 ± 0.0058	0.0259 ± 0.0012
I-Max w. GP	96.28 ± 0.19	<b>0.0223</b> ± 0.0018	<b>0.0052</b> ± 0.0029	0.1206 ± 0.0061	0.0259 ± 0.0012

Table S21: Tab. 2 Extension: CIFAR10 - DenseNet

Calibrator	Acc <sub>top1</sub> ↑	cwECE <sub><math>\frac{1}{K}</math></sub> ↓	top1 ECE ↓	NLL	Brier
Baseline	96.65 ± 0.09	0.0404 ± 0.0010	0.0253 ± 0.0009	0.1564 ± 0.0075	0.0259 ± 0.0007
5k Calibration Samples					
BBQ [19]	96.75 ± 0.19	0.0245 ± 0.0030	0.0170 ± 0.0022	0.1806 ± 0.0105	0.0279 ± 0.0010
Beta [11]	96.81 ± 0.10	0.0468 ± 0.0003	0.0154 ± 0.0013	0.1151 ± 0.0042	0.0234 ± 0.0007
Isotonic Reg. [30]	96.84 ± 0.08	0.0236 ± 0.0022	0.0140 ± 0.0024	0.1501 ± 0.0137	0.0241 ± 0.0007
Platt [21]	96.82 ± 0.11	0.0459 ± 0.0007	0.0141 ± 0.0010	0.1154 ± 0.0040	0.0233 ± 0.0007
VUC [13]	88.72 ± 0.05	0.0160 ± 0.0049	0.0643 ± 0.0059	0.2213 ± 0.0063	0.0868 ± 0.0017
Vec Scal. [12]	<b>96.84</b> ± 0.14	0.0413 ± 0.0014	0.0223 ± 0.0010	0.1373 ± 0.0077	0.0249 ± 0.0007
Mtx Scal. [12]	96.73 ± 0.09	0.0402 ± 0.0017	0.0245 ± 0.0008	0.1531 ± 0.0081	0.0257 ± 0.0007
1k Calibration Samples					
TS [5]	96.65 ± 0.10	0.0425 ± 0.0005	0.0169 ± 0.0010	0.1186 ± 0.0051	0.0237 ± 0.0006
GP [26]	96.66 ± 0.09	0.0490 ± 0.0022	0.0135 ± 0.0025	<b>0.1143</b> ± 0.0048	<b>0.0228</b> ± 0.0007
Eq. Mass	88.80 ± 0.47	0.0233 ± 0.0024	0.0637 ± 0.0023	0.2694 ± 0.0274	0.0881 ± 0.0033
Eq. Size	96.64 ± 0.22	0.0262 ± 0.0035	0.0101 ± 0.0035	0.2465 ± 0.0543	0.0256 ± 0.0003
I-Max	96.59 ± 0.32	0.0261 ± 0.0025	0.0098 ± 0.0027	0.1208 ± 0.0044	0.0239 ± 0.0005
Eq. Mass w. TS	88.80 ± 0.47	0.0234 ± 0.0026	0.0626 ± 0.0023	0.2102 ± 0.0051	0.0877 ± 0.0030
Eq. Mass w. GP	88.80 ± 0.47	0.0233 ± 0.0026	0.0634 ± 0.0025	0.2098 ± 0.0053	0.0880 ± 0.0030
Eq. Size w. TS	96.75 ± 0.10	0.0250 ± 0.0011	0.0133 ± 0.0014	0.1657 ± 0.0056	0.0249 ± 0.0007
Eq. Size w. GP	96.77 ± 0.10	0.0242 ± 0.0022	0.0050 ± 0.0012	0.1612 ± 0.0048	0.0245 ± 0.0005
I-Max w. TS	96.81 ± 0.15	0.0229 ± 0.0016	0.0125 ± 0.0017	0.1224 ± 0.0056	0.0239 ± 0.0007
I-Max w. GP	96.81 ± 0.15	<b>0.0218</b> ± 0.0012	<b>0.0048</b> ± 0.0009	0.1173 ± 0.0054	0.0231 ± 0.0005